INSPIRING EXCELLENCE

Influence of Mn Substitution on Structural and AC Magnetic Properties of $(Ni_{0.4}Cu_{0.15}Zn_{0.45})_{1-x}Mn_xFe_2O_4$ with x=0.00, 0.15

Thesis submitted to

The Department of Mathematics and Natural Sciences, BRAC University in partial fulfillment of the requirements for the award of the Degree of Bachelor of Science in Applied Physics and Electronics

By

AFRIN JAHAN SHARA

DEPARTMENT OF MATHEMATICS AND NATURAL SCIENCES

BRAC UNIVERSITY

STUDENT ID : 14115003

SESSION : Fall 2017

CANDIDATE'S DECLARATION

It is hereby declared that this thesis or any part of it has not been submitted elsewhere for the award of any degree or diploma.

Afrin Jahan Shara

ID: 14115003

Certified by

Dr. A.K.M Akther Hossain

Professor

Department of Physics, BUET

ACKNOWLEDGEMENTS

I firstly express all of my admiration to the Almighty Allah, the most beneficial, the most merciful who has enabled me to perform this research work and to submit this thesis.

I express my profound gratitude to my honorable supervisor Prof. Dr. A.K.M Akhter Hossain, Department of Physics, BUET, for his constant direction constructive criticisms and, inspiration in pursuing the whole investigation of the present research. Thanks to BUET authority for allowing me to work in the Solid State Physics Lab in BUET. The current research fellows of the lab has been ever cooperating and helpful in providing me with the all the help I needed during my work.

I am deeply grateful to the honorable Chairman of Department of Mathematics and Natural Sciences, Prof. Dr. A F M Yusuf Haider for his kind permission to let me do this work and to the honorable Ex-Chairman of Department of Mathematics and Natural Sciences, Prof. Dr. A.A. ZiaUddin Ahmed for granting me with this opportunity.

Thanks to Muhammad Lutfor Rahman, honorable faculty, BRAC University for constantly coordinating my work in the entire process.

I am indebted to BRAC University for blessing me with this opportunity and providing me with enough funds to operate my research properly.

Special thanks to my fellow research partner Zarrin Tasnim Mridula without whose participation in my work this thesis would not have been possible.

Lastly, I would like to mention my family, whose constant support and motivation gave the energy to proceed with my work.

The Author

Afrin Jahan Shara

Table of Contents

Chapter 4

Results and Discussion

List of Symbols and Abbreviations

AC	Alternating current
B	Magnetic induction
$F(\theta)$	Nelson-Riley function
f_r	Resonance frequency
L_s	Self-inductance of the sample core
L_o	Inductance of the winding coil without sample
M	Magnetization
M_s	Saturation magnetization
N_A	Avogadro's number
P	Porosity
P_{intra}	Intragranular porosity
P_{inter}	Intergranular porosity
Q	Relative quality factor
T_c	Curie temperature
T_n	Néel temperature
T_s	Sintering temperature
$tan\,\delta$	Loss factor
Z	Complex impedance
μ_i	Initial Permeability
μ'	Real part of complex permeability
μ''	Imaginary part of complex permeability
x_{spin}	Intrinsic rotational susceptibility
x_w	Domain wall susceptibility
θ	Bragg's angle

LIST OF TABLES

List of Figures

ABSTRACT

Structural and AC magnetic properties of $(Ni_{0.4}Cu_{0.15}Zn_{0.45})_{1-x}Mn_xFe_2O_4$ (x=0.00 and 0.15) have been investigated which were prepared by solid state reaction method. Various chemical compositions were calcined at 950^0C and samples of these compositions were sintered at 1100, 1150 and 1200^0C in air for 5 hours. The X-ray diffraction analysis, SEM (Scanning Electron Microscopy) and EDS (Energy Dispersive Spectroscopy) results were performed on the samples sintered at 1100^0C. X-ray diffraction pattern confirms the formation of single phase spinel structure and the lattice parameter increased with Mn^{2+}. The compositions showed a decrease in bulk and theoretical density with increase of Mn^{2+} content that can be explained by the atomic weights of the doped and substituted elements. It is also observed that porosity increases, while gain size decreases with increasing of Mn^{2+} content. EDS report showed the homogeneous distribution of elements in the samples. The real part of permeability is always higher for all temperatures when Mn is absent from the compositions. With content increment, real and imaginary part of permeability decreased. Natural resonance frequency is noticed to be decreased with rising temperature for a particular value of x. It increased with increasing Mn^{2+} content.

CHAPTER 1

Introduction

1.1. General Introduction

In the past decades, a lot of experiments have been done on Ni-Cu-Zn ferrite series to explore more about the properties they inherit due to different element or compound substitution. Today the interest regarding the series is piqued because they show an all-round performance in magnetic or electrical applications. Ferrites have always gotten preference in engineering and technology because they own magnetic moment below Curie temperature and also very useful in microwave devices and computer memory core elements as they do not undergo high eddy current losses [1]. The relative permeability of iron is about 280000, whereas copper, manganese and zinc has relative permeability close to 1, Nickel, being a ferromagnetic material has a permeability of 600[2-4]. They lack high permeability and flux density compared to iron that is mostly used for high magnetic field applications like generators, motors and power transformers [1]. However, researches and experiments are still going on how to make ferrites more permeable and to work in high frequencies for delicate and sophisticated instruments using these elements and their different combinations. These types of ferrites provide durability, high temperature endurance and small size which is exactly why Ni-Cu-Zn ferrites are immensely popular. They fulfill the requirements for delicate, advanced and high performance electronic devices.

A number of analyses regarding different material substitution in Ni-Cu-Zn ferrites are investigated by many scientists [5-11]. Gawas et al studied the influence of Mn substitution in Mössbauer and magnetic properties of Ni-Zn ferrites, enhancement of initial permeability due to Mn substitution in Ni-Zn ferrites was demonstrated by Akther et al, observation on Mg doped Ni-

Cu-Zn composition was done by Roy et al . These are the proofs that people are trying more, getting more good results through experiments which are influencing more people to study ferrites and extract the maximum benefits [5-7].

1.2. Objective of the Research

It is very visible that within a decade how memory storage chips have changed in both shape and performance, how a tiny phone is taking place of a computer by operating at high frequency and multi-functional tasks. This is the age of technology that demands high performance. As Mn has high permeability, our objective of the research is to find out what effects take place due to Mn substitution in Ni-Cu-Zn ferrite on structural, magnetic and electrical properties.

1.3. Possible Outcome of the Research

Permeability of the ferrite sample is expected to increase because it is being doped with Mn. Other than that, enhancement of grain size, less porosity and impurity may be achieved from the experiment.

1.4. Summary of the Thesis

Summary of the thesis is as follows:

Chapter 1-Introduction and objective of the research

Chapter 2-Provides basic information on ferrites, their structures and permeability mechanism

Chapter 3-Details of sample preparation and experimental techniques

Chapter 4-Includes results and discussion

Chapter 5-Conclusions and recommendations for future research.

CHAPTER 2

Literature Review

2.1. Ferrites

Ferrites are considered to be a group of ceramic like non-metallic compounds of ferric oxide with one or more other metals in different combinations that show a number of physical, chemical, electrical and magnetic properties which are extremely crucial in the field of technology and microelectronic devices. They are hard, brittle, iron containing, polycrystalline and ferrimagnetic. Saturation magnetization, high electrical resistivity, low electrical losses, and chemical stability- such characteristics make ferrite a demandable material. The general formula of ferrite is $MeO.Fe_2O_3$ where Me is any metals (Ni, Cu, Zn, Mn, Mg etc.) that forms divalent ions. Many scientists have come up with a lot of investigation on ferrites and their properties. Snoek's work particularly focuses on the high permeability of ferrites that was a combination of different metals with ferric oxides in the form of $MeZnFe_2O_4$ [12]. His work is one of the oldest research on ferrites. Current researches include the study of La^{3+} substitution on structure, surface morphology and magnetic properties of Ni-Zn ferrite, synthesis of pure and mixed nickel-cobalt ferrite, investigation on structural, dielectric and electrical properties of Zn substituted Li-Ni ferrite[11,13-14].

2.2. Spinel Structure

Ferrite has spinel structure similar to the mineral spinel of $MgO.Al_2O_3$ which is also known as cubic spinel. Spinel structure is usually consists of cubic close packed oxides with two tetrahedral and four octahedral sites per unit formula and has formula of $AO.B_2O_3$ or AB_2O_4 where A and B

represent the divalent metal (A^{2+}) and the trivalent (B^{3+}) cations respectively [15]. All A^{2+} ions occupy the tetrahedral sites and all B^{3+} ions occupy the octahedral sites. In figure 2.1 a simple spinel structure is given of the mineral spinel magnesium-aluminum. Considering a single unit of the spinel, A site is shown in the middle surrounded by four oxygen atoms in a tetrahedral structure, and B site is surrounded by 6 nearing oxygen neighbors who form an octahedral site. Thus the total structure is a repeating array of the lattices containing two tetrahedral and four octahedral sites. In total a single unit consists of eight sub cells with 8 A sites, 16 B sites, and 32 oxygen ions. In figure 2(b) a tetrahedral and octahedral structure of are shown. When chemical bonding happens, metal ions enter the A site. The void in between the oxygen ions play an important role whether to accommodate a bigger or smaller ion. If the size of the ion is bigger than the size of the intermolecular distance between two oxygens then it may possible that metal ions may not occupy the A site properly. As the oxygen ions are closely packed together, the metal ions often move the oxygen ions slightly to make rooms for their own. These oxygen ions push the surrounding octahedral sites the same amount. As a result while the tetrahedral site expands, the size of the octahedral site lessens.

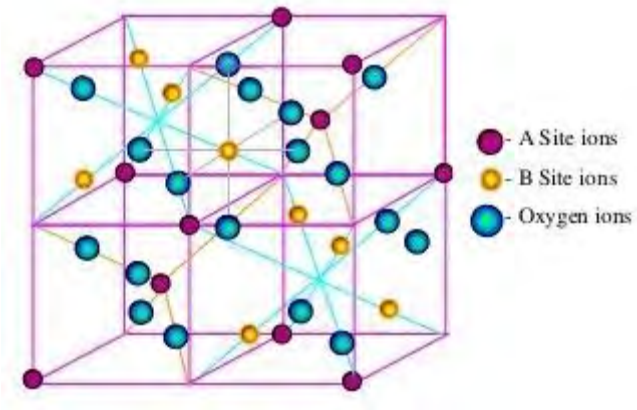

Fig 2.1: Crystal structure of spinel ferrite

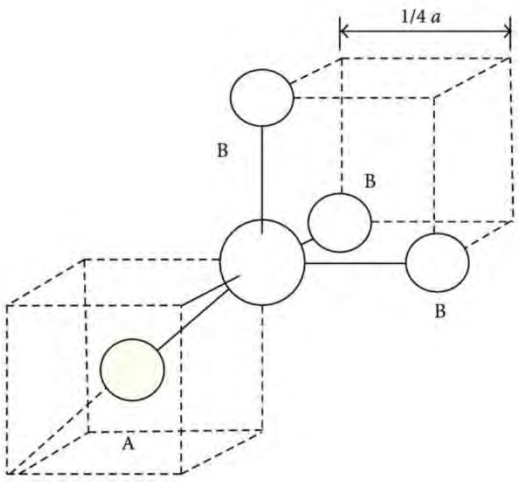

Fig 2.2: A and B site around an oxygen

2.3. Magnetic Moment of Electron

All sorts of materials have magnetic moments according to their alignment of electron spins. If an object is placed in an external magnetic field, it feel a torque to align its spins in the direction of the external magnetic field. Magnetic moment is the quantity that indicates the torque for which the object tends to produce its own magnetic field. Starting from a tiny electron to a huge planet- all has magnetic fields. Especially in the case of electron spin 'magnetic moment' is used instead of magnetic field that has both magnitude and direction. It can be compared to a current loop. When current flows in a wire loop, it produces magnetic field and the direction the magnetic field depends on the direction of the current flow. (Right hand rule).The magnetic moment (μ_c) of the loop is

$$\mu_c = I \int dS \tag{2.1}$$

Where, I=Current in the loop (A)

S=Surface area (m^2)

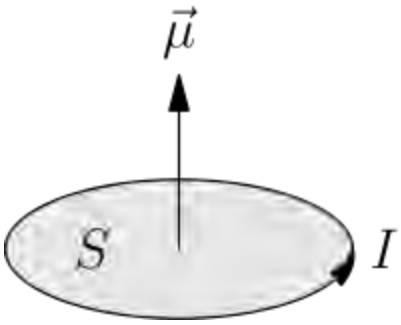

Fig 2.3: Moment in a current loop

We know current is nothing but flow of electrons. Let's consider two electrons in an orbital. Their magnetic dipole moment is caused by the rotation and electric charge which is given by

$$\mu_B = \frac{e\hbar}{2m_e} \tag{2.2}$$

μ_B is known as Bohr magneton.

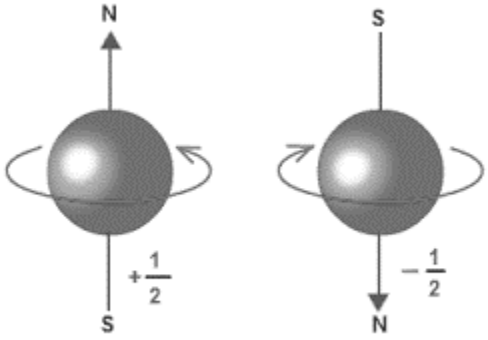

Fig 2.4: Electron spin and direction

Figure 2(d) represents a system of two electrons that both have a spin of half but in different direction. Due to the opposite direction the electrons produce magnetic fields just like the current

loop having same magnitude but in the opposite direction, one electron eliminates the other one, nullifying the total magnetic field into zero.

2.4. Classification of Magnetic Materials

When a material is placed in an external magnetic field, it feels a torque that tries to bend, distort or rearrange its electron spin configuration. This effect is known as Faraday's law of induction. This effect along with a number of other factors like atomic and molecular structure of the material, paired or unpaired electrons play a crucial role on how a material will behave and how their spins will be arranged in which manner if they are placed in a magnetic field. Depending on the spin orientation magnetic materials have been divided into five major groups. Each group represents special configuration of electron spins and therefore, show different magnetic properties.

2.4.1. Paramagnetism

These substances are poorly magnetized by an external field in the same direction of the applied field. Although they are attracted toward magnets, however they also lose their magnetic attributes once the field is removed. Unlike diamagnetic materials they have permanent magnetic moments due to some unpaired electrons in partially filled orbitals. These moments interact with each other weakly and randomly orient in different directions. That gives a very small net magnetic moment and a very small but positive value of susceptibility. Chromium, aluminum, alkali and alkaline earth metals are some known paramagnetic materials. Their susceptibility (X) is inversely proportional to temperature (T) and follow the Curie-Weiss law,

$$X = \frac{C}{T-\theta} \tag{2.3}$$

Where,

C is the curie constant

θ is a specific temperature for magnetic materials

For paramagnetic case, θ is zero [16].

It means when the temperature increases, it becomes harder to hold the spin alignment in the same direction. The thermal agitation becomes more impulsive to destroy the spin orientation completely.

2.4.2. Diamagnetism

Diamagnetic materials are those who have a nature to be magnetized very weakly by an applied magnetic field but in the opposite direction. They are repelled by the magnetic field and do not retain magnetic properties once the field is removed. For example, bismuth, antimony, water, alcohol, argon, copper, mercury, gold, tincture are diamagnetic materials. Diamagnetic materials have this wonderful feature to levitate in air to resist the field that is imposed on them. They have all paired electrons per atom for which the entire magnetic moment of the material is zero, therefore, show no tendency to be attracted by even a powerful magnet. On the contrary, they are repelled as they induce dipole moments in such way that it works in the opposite direction. Another property of the material is that they are independent of temperature [17] and have the negative magnetic susceptibility, given by

$$X = \mu_r - 1 \tag{2.4}$$

Where susceptibility X is in between the order of -10^{-6} to -10^{-5}. Figure 2(e) shows the spin orientation of magnetic materials in the absence and presence of external magnetic field.

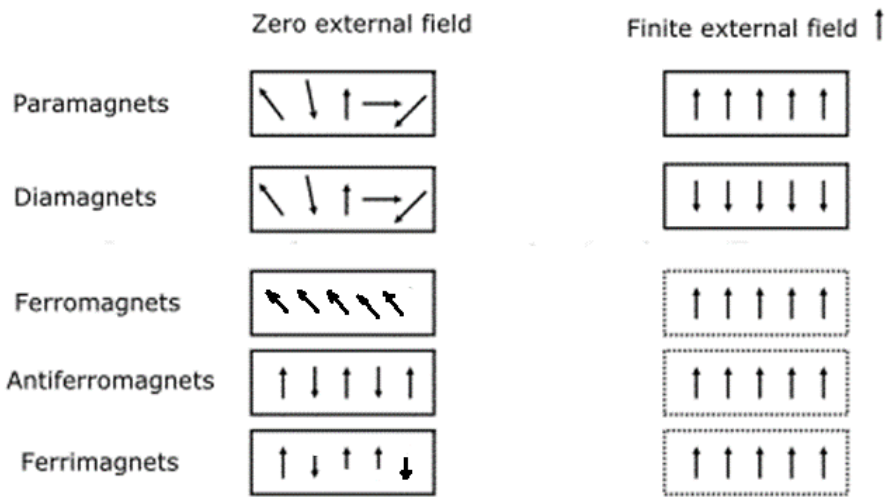

Fig 2.5: Spin orientation of different magnetic materials in a domain

2.4.3. Ferromagnetism

Ferromagnets are easily magnetized by the application of magnetic field. They tend to align their spins in the direction of the magnetic field and have this unique feature of retaining the magnetic properties even after the field is removed. They have unpaired electrons in orbitals that interacts with each other strongly and such atomic structure supports them to align their spin in the same direction of the magnetic field. They are used to make permanent magnets. They get their strong magnetic behavior because of the magnetic domains. In these domains, spins are aligned in the same direction within the domains to gain a large amount of magnetic moments so that the moment of individual domain is strong, but the net moment of all the domains is zero [17]. They have high permeability in the order of 10^3 to10^5 and high susceptibility (way more than diamagnetic and paramagnetic) that varies along with temperature. All ferromagnets have a maximum temperature above which they lose their spin orientation because of thermal agitation. It is known as the Curie temperature when achieved, the ferromagnets lose their magnetic abilities.

2.4.4. Antiferromagnetism

Antiferromagnetic materials are those who have anti parallel alignment of electron spins between neighboring electrons to cancel each other's moments much like the paramagnetic materials. The only element that shows this kind of behavior is chromium in the room temperature. Antiferromagnetic materials own a specific temperature called Neel temperature above which their antiferromagnetism property disappears.

2.4.5. Ferrimagnetism

Ferrimagnetism belong to a group of compounds those having exchange interactions leading to parallel alignments of atoms in some sights and anti-parallel alignments of atoms in some sights [18]. They have similarities with ferromagnetic materials having lower saturation magnetizations. Ferrimagnetism has characteristics like spontaneous magnetization like ferromagnets and above Curie temperature they have zero magnetic order like paramagnets. They have high resistivity and anisotropy which are proving to be very useful in the technological applications.

2.5. Domain Theory in Magnetism

The domain theory explains why ferromagnets can retain their properties even after removing magnetic field. Ferromagnets are divided into some very small region that own a group electrons having the same direction within the same domain. These domains are about 10^{-12} to 10^{-8} m^3 in size. The interaction within one domain is so strong that they produce a net moment although it gets cancelled by the moment which is created by another domain. Ferromagnets contain millions of domain like these making the total magnetic flux zero. When a strong magnetic field is applied, the spin directions of all domain get aligned producing a humongous net magnetic flux that tries

to keep the alignment same even after removing the field, however, the alignment may shift a little which is shown by the figure below. This result is explained by the hysteresis curve, why ferromagnets do not follow the same path of magnetization with increasing and decreasing of magnetic field which is known as the remnant magnetization.

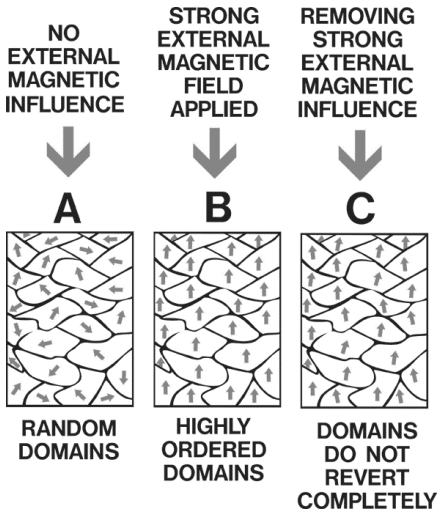

Fig 2.6: Domains in different field conditions

2.6. Microstructure

Microstructure is basically the arrangements of phases and defects within a material in nm length scale obtained using microscope. Microstructure are formed when a material under goes by phase transition through sintering or pressurizing, deforming etc. Microstructure study is pivotal in ferrite composition because to a great extent, the physical properties of the material is driven by microstructure or more specifically the grain boundaries. Grain boundary is the region of interface between two grains of the same phase in a polycrystalline material. Grains are formed of atoms that share lose bonds with each other within that grain. When stress is applied, the bond between the atoms are pulled apart forming dislocations gradually appearing as grain boundary.

Porosity, a common term that appears with microstructure of crystallography, it is the void or empty space in a crystal structure. There are two types of porosity seen in grain size.

a) Intergranular and b) Intragranular porosity. Intragranular occurs within a grain and intergranular occurs in between grains.

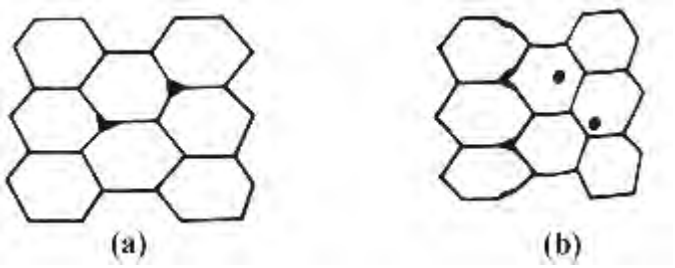

Fig 2.7: a) intergranular porosity, b) intragranular porosity

2.7. Theories of Permeability

One of the primary objectives of studying ferrites is to obtain such material composition that has high permeability with low loss. Permeability indicates the degree of magnetization or magnetic field induction *B* of a material in an applied field intensity *H* [19, 20]. Permeability is given by,

$$B = \mu H \tag{2.5}$$

μ is the proportional constant between the induced and applied field.

If the applied field is very low, approaching to zero, the ratio then called the initial permeability and written as,

$$\mu_i = \frac{\Delta B}{\Delta H}_{(\Delta H \to 0)} \tag{2.6}$$

If a magnetic field is subjected to an AC magnetic material, we get

$$B = B_0 e^{i\omega t} \tag{2.7}$$

It is observed that the magnetic flux density *B* experiences a delay which is caused due to the presence of various losses and is thus expressed as,

$$B = B_0 e^{i(\omega t-\delta)} \tag{2.8}$$

Where, δ is the phase angle and indicates the delay of *B* with respect to *H*. The permeability is then given by

$$\mu = \frac{B}{H} = \frac{B_0 e^{i(\omega t-\delta)}}{H_0 e^{i\omega t}} = \frac{B_0 e^{-i\delta}}{H_0} = \frac{B_0}{H_0}\cos\delta - i\frac{B_0}{H_0}\sin\delta = \mu^{/} - i\mu^{//}$$

Where, $$\mu^{/} = \frac{B_0}{H_0}\cos\delta \tag{2.9}$$

and $$\mu^{//} = \frac{B_0}{H_0}\sin\delta \tag{2.10}$$

The real part ($\mu^{/}$) of the complex initial permeability represents the component of *B* that is in phase with *H*, so it corresponds to the normal permeability. If there are no losses we should get $\mu=\mu^{/}$. The imaginary part ($\mu^{//}$) is the component that lags behind *H* by the phase angle. The presence of such a component requires supply of energy to maintain the alternating magnetization, regardless of the origin of delay. It is useful to introduce the loss factor $\tan\delta$ the ratio of $\mu^{//}$ to $\mu^{/}$ which can be obtained by,

$$\frac{\mu^{//}}{\mu^{/}} = \frac{\frac{B_0}{H_0}\sin\delta}{\frac{B_0}{H_0}\cos\delta} = \tan\delta \tag{2.11}$$

This $\tan\delta$ is called loss factor.

The quality factor is defined as the reciprocal of this loss factor, i.e.

$$\text{Quality factor} = \frac{1}{\tan\delta} \tag{2.12}$$

And the relative quality factor,

$$Q = \frac{\mu'}{\tan\delta}$$

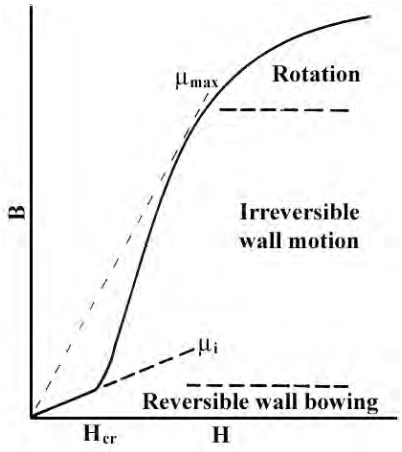

Fig 2.8: Schematic magnetization curve showing the important parameter: initial permeability, μ_i (the slope of the curve at low fields) and the main magnetization mechanism in each magnetization range.

The graph illustrates the behavior of both μ' and μ'' with frequency are called the complex permeability spectrum of the material [21].The measurement of complex permeability gives us valuable information about the nature of domain wall and their movements. In dynamic measurements the eddy current loss is very important that occurs due to the irreversible domain wall movements. The permeability of a ferrimagnetic substance is the combined effect of the wall permeability and rotational permeability mechanisms.

2.8. Mechanism of Permeability

The mechanisms can be explained as follows: A demagnetized magnetic material is divided into number of Weiss domains separated by Bloch walls. In each domain all the magnetic moments are oriented in parallel and the magnetization has its saturation value M_s. In the walls the magnetization direction changes gradually from the direction of magnetization in one domain to that in the next. The equilibrium positions of the walls result from the interactions with the magnetization in neighboring domains and from the influence of pores; crystal boundaries and chemical inhomogeneities which tend to favor certain wall positions.

2.9. Wall Permeability

The mechanism of wall permeability arises from the displacement of the domain walls in small fields. Let us consider a piece of material in the demagnetized state, divided into Weiss domains with equal thickness L by means of 180° Bloch walls as shown in figure 2.9. The walls are parallel to the YZ plane. The magnetization M_s in the domains is oriented alternately in the $+Z$ or $-Z$ direction. When a field H with a component in the $+Z$ direction is applied, the magnetization in this direction will be favored. A displacement dx of the walls in the direction shown by the dotted lines will decrease the energy density by an amount [22, 23]:

$$\frac{2M_s H_z dx}{L}$$

This can be described as a pressure $M_s H_z$ exerted on each wall. The pressure will be counteracted by restoring forces which for small deviations may assume to be kdx per unit wall surface. The new equilibrium position is then given by

$$d = \frac{M_s H_z dx}{L}$$

From the change in the magnetization

$$\Delta M = \frac{2M_s d}{L},$$

The wall susceptibility χ_w may be calculated. Let H makes the angle θ with Z direction. The magnetization in the θ direction becomes

$$(\Delta M)_\theta = \frac{2M_s d}{L}\cos\theta, \text{ And with } H_z = H\cos\theta \text{ and } d = \frac{2M_s H_z}{K}$$

We obtain

$$\chi_w = \frac{(\Delta M)_\theta}{H} = \frac{4M_s^2 \cos^2\theta}{KL}$$

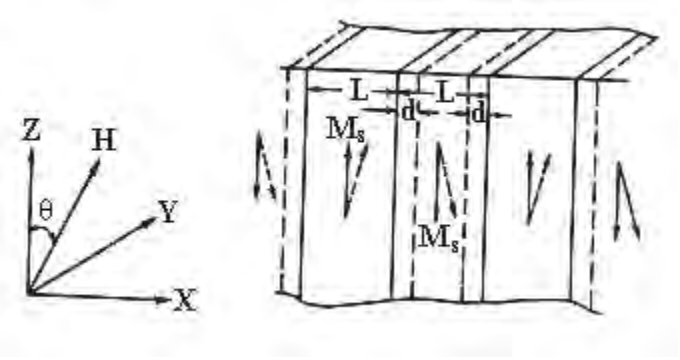

Fig 2.9: Magnetization by wall motion and spin rotation.

2.10. Rotational Permeability

The rotational permeability mechanism arises from rotation of the magnetization in each domain. The direction of M can be found by minimizing the magnetic energy E as a function of the orientation. Major contribution to E comes from the crystal anisotropy energy. Other contributions may be due to the stress and shape anisotropy. The stress may influence the magnetic energy via the magnetostriction. The shape anisotropy is caused by the boundaries of the sample as well as by pores, nonmagnetic inclusions and inhomogeneities. For small angular deviations, α_x and α_y may be written as

$$\alpha_x = \frac{M_x}{M_s} \text{ and } \alpha_y = \frac{M_y}{M_s}.$$

For equilibrium Z -direction, E may be expressed as [24, 25]

$$E = E_0 + \frac{1}{2}\alpha_x^2 E_{xx} + \frac{1}{2}\alpha_y^2 E_{yy}$$

Where it is assumed that x and y are the principal axes of the energy minimum. Instead of E_{xx} & E_{yy}, the anisotropy field H_x^A and H_y^A are often introduced. Their magnitude is given by

$$H_x^A = \frac{E_{xx}}{2M_s} \text{ and } H_y^A = \frac{E_{yy}}{2M_s},$$

H_x^A & H_y^A represent the stiffness with which the magnetization is bound to the equilibrium direction for deviations in x and y direction, respectively. The rotational susceptibilities $\chi_{r,x}$ and $\chi_{r,y}$ for fields applied along x and y directions, respectively are

$$\chi_{r,x} = \frac{M_s}{H_x^A} \text{ and } \chi_{r,y} = \frac{M_s}{H_y^A}.$$

For cubic materials it is often found that H_x^A and H_y^A are equal. For $H_x^A = H_y^A = H^A$ and a field H which makes an angle θ with the Z direction the rotational susceptibility, $\chi_{r,c}$ in one crystallite becomes

$$\chi_{r,c} = \frac{M_s}{H^A} \sin^2 \theta$$

A polycrystalline material consisting of a large number of randomly oriented grains of different shapes, with each grain divided into domains in a certain way. The rotational susceptibility χ_r of the material has to be obtained as a weighted average of $\chi_{r,c}$ of each crystallite, where the mutual influence of neighboring crystallites has to be taken into account. If the crystal anisotropy dominates other anisotropies, then H^A will be constant throughout the material, so only the factor $\sin^2 \theta$ has to be averaged. Snoek [25] assuming a linear averaging of $\chi_{r,c}$ and found

$$\chi_r = \frac{2M_s}{3H^A}$$

The total internal susceptibility

$$\chi = \chi_w + \chi_r = \frac{4M_s^2 \cos^2 \theta}{KL} + \frac{2M_s}{3H^A}$$

If the shape and stress anisotropies cannot be neglected, H^A will be larger. Any estimate of χ_r will then be rather uncertain as long as the domain structure, and the pore distribution in the material are not known. A similar estimate of χ_w would require knowledge of the stiffness parameter k and the domain

width L . These parameters are influenced by such factors as imperfection, porosity and crystallite shape and distribution which are essentially unknown.

CHAPTER 3

Sample Preparation and Experimental Techniques

This chapter provides an overview of the sample preparation and methods that have been used to determine different parameters of the ferrites.

3.1. Chemical Composition of Studied Samples

In this present work, the compositions of Mn^{2+} doped $(Ni_{0.4}Cu_{0.15}Zn_{0.45})_{1-x}Mn_xFe_2O_4$ were synthesized and investigated. The samples were:

$(Ni_{0.4}Cu_{0.15}Zn_{0.45})_{1-x}Mn_xFe_2O_4$ (with x=0.00, 0.15)

3.2. Various Methods for Preparing Samples

There are a number of methods which are followed to study ferrites and their compositions. Among these, the conventional ceramic process and solid state reaction method are widely used to prepare ferrite powder. Other methods are [26, 27],

1) Sol-gel synthesis

2) Co-precipitation

3) Organic precursors

4) Freeze dying

5) Spray dying

6) Combustion synthesis

7) Glass crystallization

For this experiment, solid state method reaction method is used which is described thoroughly below

3.3. Solid State Reaction Method

Solid state reaction method consists of several steps to get the final products which are been studied. Solids do not react at room temperature over normal time scales for which it is necessary to heat them at higher temperature to complete chemical reaction. This reaction depends on factors such as structural properties of the reactants, surface area of the solids, reactions conditions and their thermodynamics [26].

The required composition is usually prepared from the appropriate amount of raw materials of oxides or carbonates by crushing, grinding and milling.

Once the powders are finely ground, they are calcined in air for 5 hours at temperature above 500^0C. Calcine temperature may vary according to needs. The calcination process makes the impurities go away. The calcined powders are then again hand milled to ensure they are properly smoothed. The necessary pellets and toroid samples are prepared from the calcined powder according to the need using die punch assembly or hydrostatic or isostatic pressure. Sintering is carried out at temperatures from 900^0C to 1600^0C for a typical time of 1 to 10 hours in different atmospheres [28, 29].

The general solid state reaction leading to a ferrite $MeFe_2O_4$ may be represented as

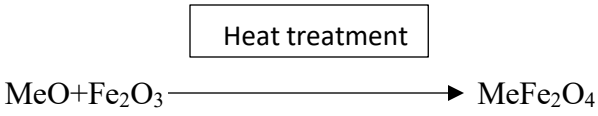

Where Me is the metal ions. There are basically four steps in the preparation of ferrites.

1) Preparation of materials to form an intimate mixture with the metal ions in the ratio which they will have in the final product.

2) Calcining the mixture to form ferrite.

3) Grinding the calcined powders and pressing to get the required shape.

4) Sintering to produce highly densified product.

3.4. Details of Calcination, Pressing and Sintering

Calcination is a process of obtaining a homogenous and phase pure composition of mixed powders by heating them for a certain amount of time at a certain temperature and then cooled down slowly. Calcination can be repeated several times to obtain a high degree of homogeneity. The calcined powders are then again crushed.

A binder is usually added prior to compaction at a concentration lower than 5wt%. Binders are polymers or waxes that is used to facilitate the particles flow during compacting and increase the bonding between particles. The most commonly used binder for ferrites is polyvinyl acid. During sintering binders decompose and are eliminated from the ferrite. Pressures are used to for compacting very widely but are commonly several tons per square inch. (i.e. up to $10\text{^}8nm^{-2}$) to desired toroid and pellet shapes.

Sintering process makes a sample more dense, tough body by heating a compacted powder for a certain period of time at high temperature enough to promote diffusion but surely below the melting point of the main component.

Below is given the process of sample preparation through by a flowchart.

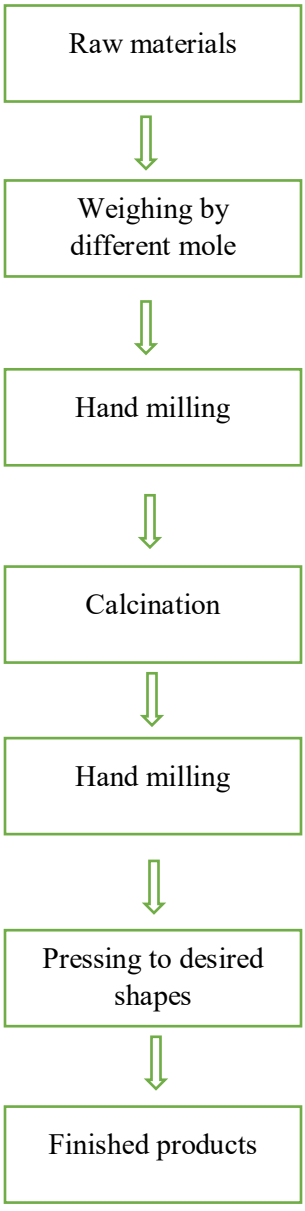

Fig 3.1: Flow chart of the stages in preparation of spinel ferrite

The purposes of sintering process are-

1) To bind the particles to impart sufficient strength to the product.

2) To densify the material and eliminating pores.

3) Gain homogeneity by completing the reactions left unfinished in calcination.

Coble and burke [29] found out the empirical relation regarding rate of grain growth which is given by

$$\bar{d}=kt^n \qquad (3.1)$$

Where $\bar{d}$ is the mean grain diameter. n is about 1/3,t is the sintering time and k is a temperature dependent parameter. Sintering is divide into 3 stages [29, 30]-

1) Contact area between particle increases.

2) Porosity changes from open to close porosity

3) Pore volume decreases and gains grow.

The following figure shows the grain growth at different sintering stages.

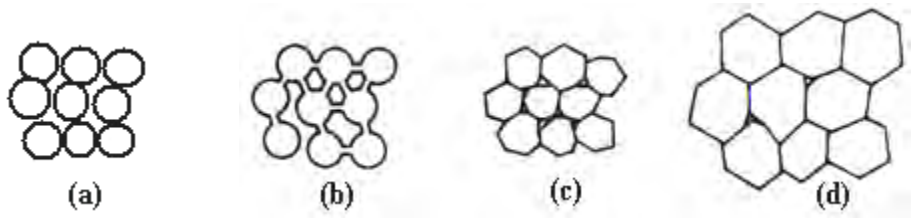

Fig 3.2: Schematic representation of sintering stages: (a) green body, (b) initial stage, (c) intermediate stage, and (d) final stage

3.5. Stoichiometric Ratio Calculation

The following tables show the calculation of different amount of raw materials that was taken to make the samples. . For the samples used in this work, each was of a total of 15 gram and each pellet and ring were made of 1 gram.

Table 3.1: Atomic mass of the compounds

Raw materials	Ni (g/mole)	Cu (g/mole)	Zn (g/mole)	Mn (g/mole)	C (g/mole)	Fe (g/mole)	O (g/mole)	Total (g/mole)
NiO	58.6934						15.9994	74.6928
Cu_2O		63.546					15.9994	143.0914
ZnO			65.38				15.9994	81.3794
$MnCO_3$				54.938	12.0107		15.9994	114.9469
Fe_2O_3						55.845	15.9994	159.6882

Table 3.2: Total mass of the sample

Value of x	Composition	Mass of the sample (g/mole)
0.00	$Ni_{0.4}Cu_{0.15}Zn_{0.45}Fe_2O_4$	58.6934*0.4+63.546*0.15+65.38*0.45+ 55.845*2+15.9994*4=238.11786
0.15	$Ni_{0.34}Cu_{0.1275}Zn_{0.3825}Mn_{0.15}Fe_2O_4$	58.6934*0.34+63.546*0.1275+65.38*0.3825+ +54.938*0.15+55.845*2+15.9994*4 =236.99402

Table 3.3: Calculation for the need of raw materials

Composition	Need of	Amount (g/mole)
$Ni_{0.4}Cu_{0.15}Zn_{0.45}Fe_2O_4$	NiO	74.6928*0.4*15/238.11786 =1.8821
	Cu_2O	143.0914*0.15*15/238.11786 =1.3521

	ZnO	81.3794*0.45*15/238.11786 =2.3069
	$MnCO_3$	0
	Fe_2O_3	159.6882*15/238.11786 =10.0594
$Ni_{0.34}Cu_{0.1275}Zn_{0.3825}Mn_{0.15}Fe_2O_4$	NiO	74.6928*0.34*15/236.994021 =1.6073
	Cu_2O	143.0914*0.1275*15/236.994021 =1.1547
	ZnO	81.3794*0.3825*15/236.994021 =1.9701
	$MnCO_3$	114.9469*0.15*15/236.994021 =1.0913
	Fe_2O_3	159.6882*15/236.994021 =10.1071

3.6. Preparation of the Sample

$(Ni_{0.4}Cu_{0.15}Zn_{0.45})_{1-x}Mn_xFe_2O_4$ (with x=0.00, 0.15) were prepared by solid state reaction method with the stoichiometric amount of raw materials. The extra pure powder (99.9%) of NiO, Cu_2O, ZnO, $MnCO_3$, Fe_2O_3 are weighted according to the required composition and hand milled for about 5 hours for chemical reaction to happen using an agitate mortar and pistol. Before using mortar and pistol, they were cleaned each and every time very carefully to avoid impurity mixing. This is facilitated further by calcination which is undertaken for 5 hours in air at a temperature of 950^0C. The calcined powders were granulated using polyvinyl acid a binder and pressed in to desired toroid and pellet shapes. In the final stage they were sintered at various temperatures from 1100^0C to 1200^0C in air for 5 hours. The temperature ramps for sintering are 5^0C /min for heating and 10^0C /min for cooling.

3.7. Experimental Techniques

In this chapter, the basic experimental techniques of measuring lattice parameter and frequency depended permeability of ferrite sample is described.

3.7.1. X-ray Diffraction

If a monochromatic radiation of wavelength λ is incident on periodic crystal plane at an angle of θ and is diffracted at the same angle as shown in the figure, the Bragg diffraction condition in given by

$$2d\,Sin\theta = n\lambda \tag{3.2}$$

Where *d* is the distance between crystal planes and *n* is the positive integer which represents the order of reflection. Equation (4.1) is known as Bragg law. This Bragg law suggests that the diffraction is only possible when $\lambda \leq 2d$. The X-ray diffraction provides substantial information of the crystal structure.

Pellets of $(Ni_{0.4}Cu_{0.15}Zn_{0.45})_{1-x}Mn_xFe_2O_4$ (with x=0.00, 0.15) sintered at 1100 is used for X-ray diffraction. The lattice parameter for each peak of each sample is calculated by the formula given below,

$$a = d\sqrt{h^2 + k^2 + l^2} \tag{3.3}$$

Where *h*, *k* and *l* are the indices of the crystal planes. To determine the exact lattice parameter for each sample, Nelson-Riley method was used. The Nelson-Riley function *F (θ)* is given as

$$F(\theta) = \frac{1}{2}\left[\left(Cos^2\theta / Sin\theta\right) + \left(Cos^2\theta / \theta\right)\right] \tag{3.4}$$

The values of all peaks is plotted against *F (θ)* of a sample. Using least square fit method, the lattice parameter a_0 is determined. The point where the least square fit straight line cut the y-axis is the actual lattice parameter of the samples.

3.7.2. Bulk Density Measurements

The physical or bulk density of the samples were determined by the formula,

$$\rho_B = \frac{M}{V} \tag{3.5}$$

Where ρ_B is the bulk density, M is the wright of the sample and V is the volume. V was determined by calculating the radius and thickness of the pellet and then put into the formula,

$$V = \pi r^2 h$$

The theoretical density is calculated by using the following expression

$$\rho_{th} = \frac{8M}{N_A a_o^3} g/cm^3 \tag{3.6}$$

Where n is the Avogadro number (6.02×10^{23} mol^{-1}), m is the molecular weight. Porosity was calculated from the relation,

$$\{100(\rho_{th} - \rho_B)/\rho_{th}\}\% \tag{3.7}$$

3.7.3. Study of Microstructure

Microstructure of the ferrite composition shows the grain size of the sample which is sintered at 1100^0C.The samples were observed under high resolution optical microscope and photographed. Grain diameters were determined by liner intercept technique for which several random horizontal and vertical lines were drawn on the micrographs. Therefore the number of grains were counted that intersected and measured the length of the grains along the line traversed. Finally the grain size was calculated.

3.7.4. Complex Permeability Measurement

Permeability is a quantity that defines the change in self-inductance of a coil in the presence of a magnetic core. The core is taken as a toroid shape to avoid demagnetizing effects.

Complex initial permeability is given by

$$Z = R + jX = j\omega L_0 \mu = j\omega L_0 (\mu' - j\mu'')$$

Where the resistive part is,

$$R = \omega L_0 \mu^{//}$$

And the reactive part is,

$$X = \omega L_0 \mu^{/}$$

Here, L_0 is the inductance of the winding coil in air that is without loss.

μ is the permeability of the magnetic core

On the above expressions, the real part and the imaginary part were calculated by $\mu_i^{/} = L_s / L_0$ and $\mu_i^{//} = \mu_i^{/} \tan\delta$, where L_s is the self-inductance of the sample core sample core and $L_0 = \mu_o N^2 S / \pi \bar{d}$ derived geometrically.

N is the number of turns of the coil (N = 4), S is the area of cross section of the toroidal sample as given below:

$$S = d \times h,$$

Where $d = \frac{d_2 - d_1}{2}$,

$d_1 =$ Inner diameter,

$d_2 =$ Outer diameter,

$h =$ Height

And $\bar{d}$ is the mean diameter of the toroidal sample as given below:

$$\bar{d} = \frac{d_1 + d_2}{2}$$

The relative quality factor is determined from the ratio $\frac{\mu_i^{/}}{\tan\delta}$.

CHAPTER 4

Results and Discussion

4.1. X-Ray Diffraction Analysis

X-ray diffraction was done on $(Ni_{0.4}Cu_{0.15}Zn_{0.45})_{1-x}Mn_xFe_2O_4$ (with x=0.00, 0.15) that were sintered at 1100^0C in air for 5 hours to explore the spinel structure and physical properties of the samples. The results found in the experiment indicated that these materials have formed a well-defined single crystalline phase and formation of spinel structure for each composition. The positions of the peaks matched with the reported value [31]. In figure 4.1, X-ray patterns are shown for different compositions.

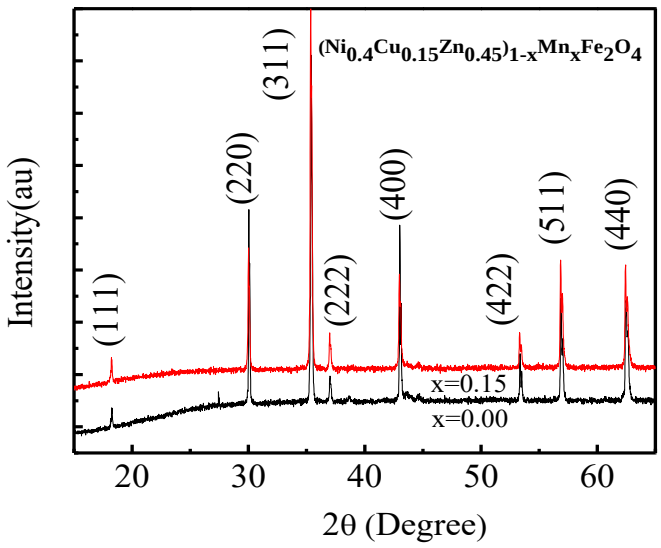

Fig 4.1:X-ray diffraction patterns for $(Ni_{0.4}Cu_{0.15}Zn_{0.45})_{1-x}Mn_xFe_2O_4$.

From the XRD report, lattice parameter is found with the help of Nelson-Riley function. In figure 4.2, the lattice parameter is shown as a function of Mn^{2+} content.

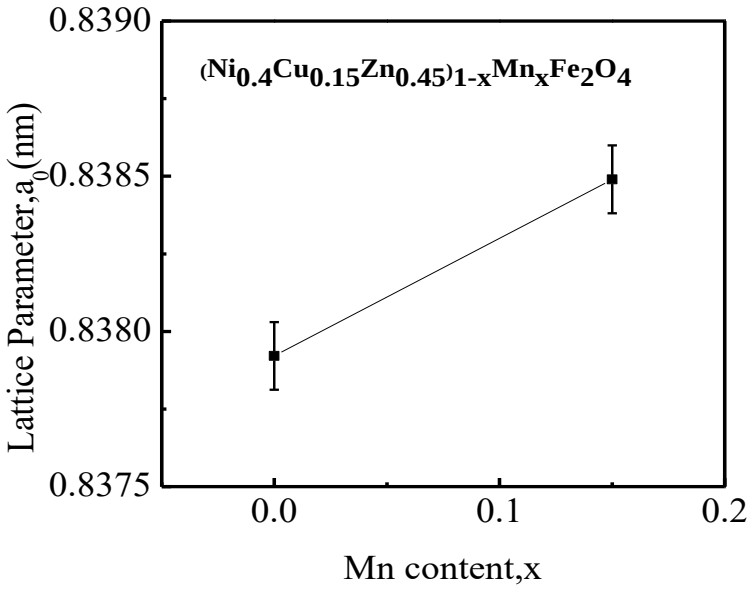

Fig 4.2: The variation of lattice parameter with Mn^{2+} for $(Ni_{0.4}Cu_{0.15}Zn_{0.45})_{1-x}Mn_xFe_2O_4$.

The parameter increases with Mn^{2+} content which can be explained in terms of ionic radii. Mn^{2+} has an ionic radius of 0.83 Å [32] which replaces Zn^{2+} (0.74 Å), Ni^{2+} (0.69Å) and Cu^{2+} (0.72Å) [31, 33]. This increment is because of the small cations are getting replaced by big cations for which the lattice parameter has increased.

4.2. Bulk Density and Porosity

Bulk density, theoretical density and porosity of various compositions of $(Ni_{0.4}Cu_{0.15}Zn_{0.45})_{1-x}Mn_xFe_2O_4$ (x=0.00, x=0.15) sintered at 1100, 1150 and 1200^0C have been calculated using the Eq-3.5, Eq-3.6, and Eq-3.7 respectively. The following figure 4.3 shows the variation of theoretical density and bulk density with increasing content of Mn^{2+} at sintering temperature of 1100^0C. The bulk density decreases with Mn^{2+} content which can be explained by the atomic weights of the elements of the ferrite composition. Mn has the atomic weight of 54.938 (amu) [34] whereas Ni, Zn and Cu have 58.6934(amu), 65.38(amu) and 63.546(amu) respectively [31]. With Mn^{2+} reducing the other cations, the total mass of the samples have also been reduced. As a result, the

bulk density has decreased .Theoretical density depends on the lattice constant and molecular mass of the samples.

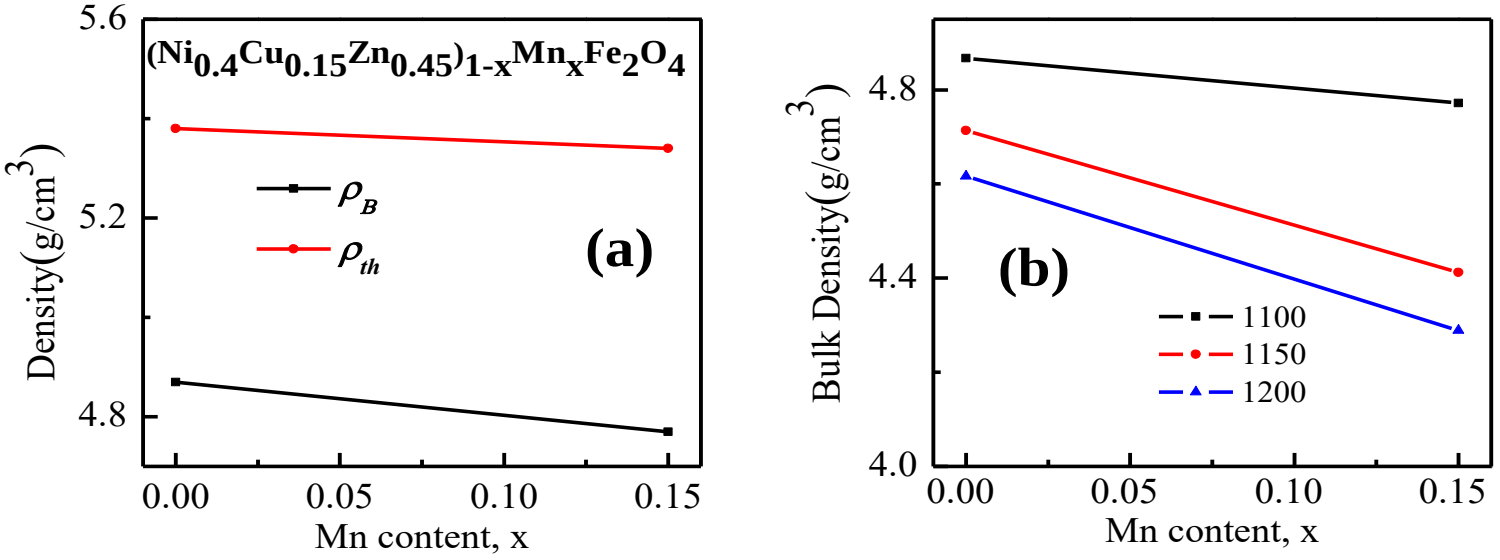

Fig 4.3: The variation of (a) Bulk and theoretical density sintered at 1100^0C and (b) Bulk density with Mn content for various $(Ni_{0.4}Cu_{0.15}Zn_{0.45})_{1-x}Mn_xFe_2O_4$ sintered at different temperature.

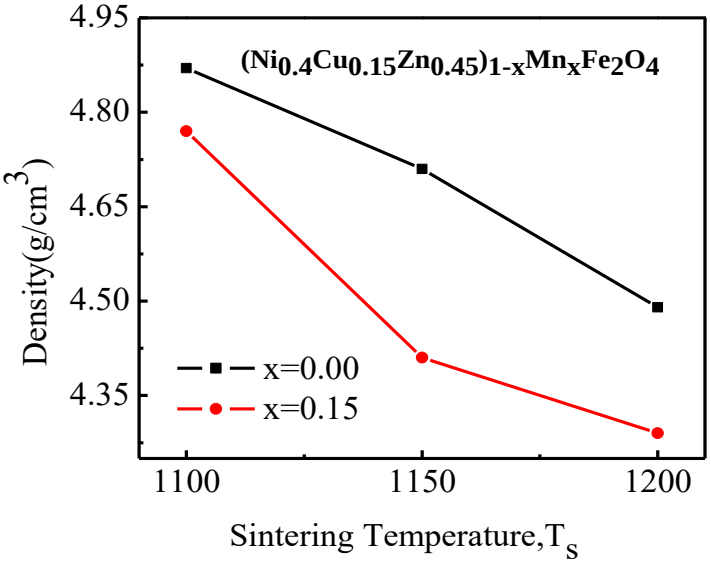

Figure 4.4: Bulk density for $(Ni_{0.4}Cu_{0.15}Zn_{0.45})_{1-x}Mn_xFe_2O_4$ sintered at different temperature, T_s.

It is evident that the theoretical densities are larger on every point than their corresponding bulk densities which may be due to pores in the samples. Another trend can be identified from the same graph which shows the theoretical density has also deceased although the lattice parameter (a_0) increased. This may be caused by Mn doping for which the total molecular mass lessened with increasing Mn^{2+} content. Similar behavior is observed by Hamid [34].

Bulk density reduction with increasing sintering temperature may be explained with the help of intragranular porosity. At high temperature the intragranular porosity is increased due to discontinuous grain growth. It rises with temperature that makes grain growth faster which eventually leaves pores trapped inside grains. Hence, results in density reduction.

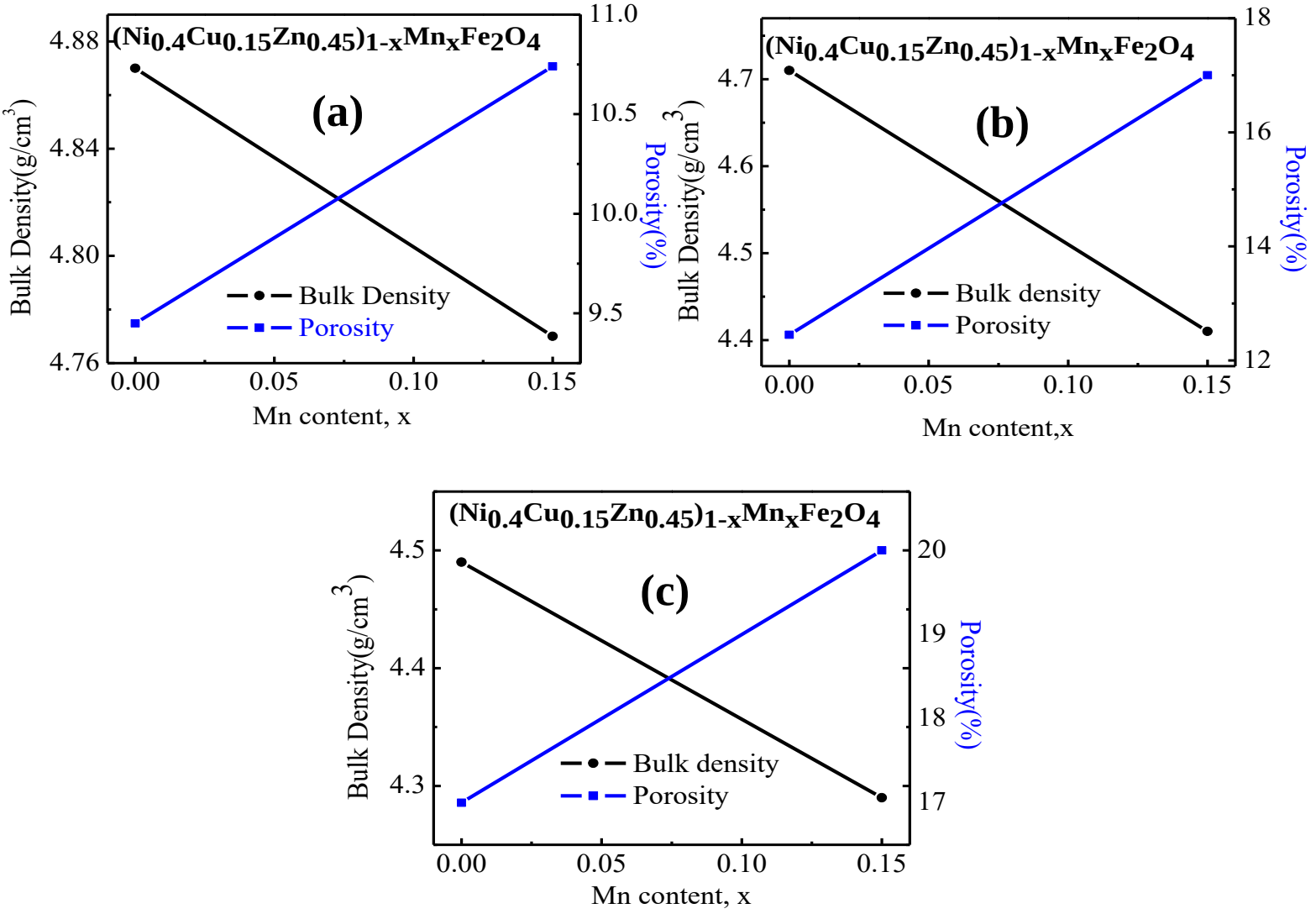

Fig 4.5: Bulk density and porosity with Mn content for $(Ni_{0.4}Cu_{0.15}Zn_{0.45})_{1-x}Mn_xFe_2O_4$ sintered at a) 1100 b) 1150 and c) 1200^0C.

4.3. Microstructural Investigation

The optical micrographs of various samples of $(Ni_{0.4}Cu_{0.15}Zn_{0.45})_{1-x}Mn_xFe_2O_4$ sintered at 1100^0C have also been observed. The following figures show the graphs of two different compositions that varies with x. The average grain size decreases with increase of Mn^{2+} that may be due to the modified chemical properties as a result of Mn^{2+} substitution. This decrease of grain size may also has resulted from the fact that each element has a different melting temperature. Mn has a melting

temperature of 1518 K [34] which is lower than Ni (1726 K) but higher than Cu (1357 K) and Zn (692 K) [31, 35].

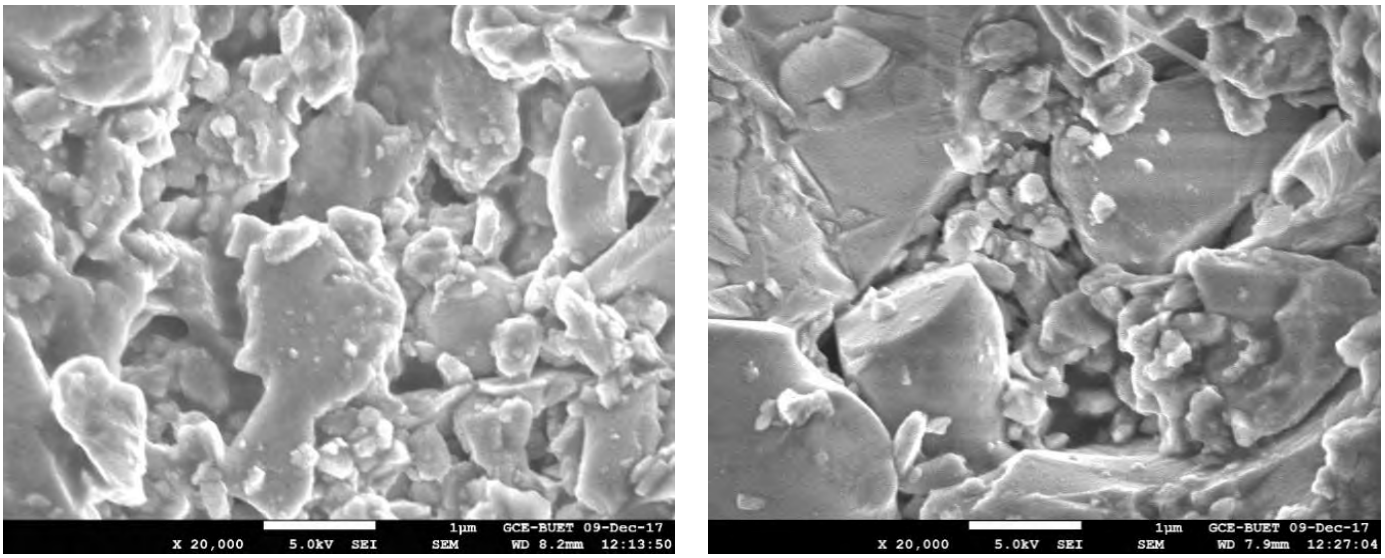

(a) x = 0.00 (b) x = 0.15

Fig 4.6: Micrographs of $(Ni_{0.4}Cu_{0.15}Zn_{0.45})_{1-x}Mn_xFe_2O_4$ sintered at 1100^0C.

During the solidification process the melting point of different elements play a crucial role that cause each compositions to attain completely different physical and chemical properties. Another reason for grain size reduction can be the increasing amount of pores and voids within grains and grain boundaries.

Table 4.1: Lattice parameter, theoretical density, bulk density, porosity, natural resonance frequency, grain size of various $(Ni_{0.4}Cu_{0.15}Zn_{0.45})_{1-x}Mn_xFe_2O_4$ at different sintering temperatures

x	a_0(nm)	$T_s(^0C)$	ρ_{th} (g/cm^3)	ρ_B (g/cm^3)	P (%)	f_r (MHz)	Grain size(μm)	μ_i' (at 10^5 Hz)
0.00	0.8379	1100	5.38	4.87	9	12.9	1.85	222
		1150		4.71	12	12.6		183
		1200		4.49	17	11.7		204
0.15	0.8385	1100	5.34	4.77	11	28.5	1.65	152
		1150		4.41	17	26.2		123
		1200		4.29	20	22.2		97

4.4. EDS

The purity and chemical composition of samples were checked using EDS analysis. Figure 4.7 and 4.8 show disparate surface points in EDS spectrum of the samples with x=0.00 and x=0.15 to conclude the homogeneity of the investigated samples. The concentrations of different constituents involved in the investigated sample at 10 KeV over various points on the surface of $(Ni_{0.4}Cu_{0.15}Zn_{0.45})_{1-x}Mn_xFe_2O_4$ with increasing Mn content are given in table 4.2. This table indicates the concentrations of different constituents are close to each other. The spectrum images reveal no trace of impurity and molar proportions of the present elements are in good agreement with that of expected values which shows there is no chemical reaction or any loss of ingredients.

View000

JEOLUSER 1/1

Title : IMG1

Instrument : 7600F
Volt : 5.00 kV
Mag. : x 30,000
Date : 2017/12/09
Pixel : 512 x 384

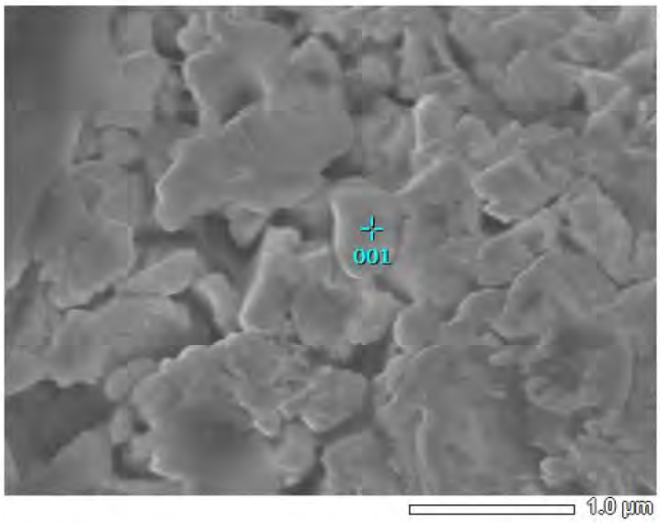

001 VFS = 1000 count

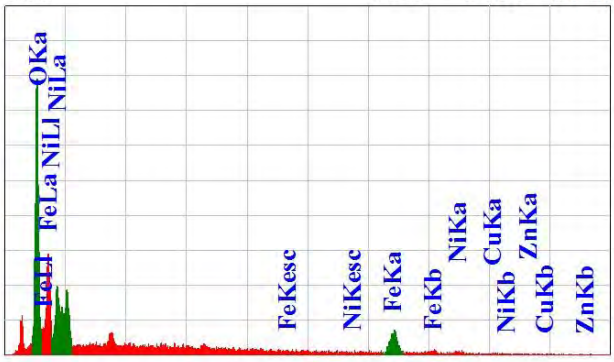

Acquisition Parameter
Instrument : 7600F
Acc. Voltage : 10.0 kV
Probe Current: 1.00000 nA
PHA mode : T3
Real Time : 30.21 sec
Live Time : 30.00 sec
Dead Time : 0 %
Counting Rate: 743 cps
Energy Range : 0 - 20 ke\

ZAF Method Standardless Quantitative Analysis
Fitting Coefficient : 0.1637

Element	(keV)	Mass%	Sigma	Atom%	Compound	Mass%	Cation	K
O K	0.525	25.75	0.34	55.89				37.0335
Fe K	6.398	34.77	1.57	21.62				41.0155
Ni L	0.851	23.94	0.90	14.16				12.5534
Cu L*	0.930	4.20	0.29	2.30				4.1929
Zn L	1.012	11.34	0.48	6.02				5.2047
Total		100.00		100.00				

JED-2300 AnalysisStation JEOL

Fig 4.7.1: EDS patterns at point 1 for x=0.00.

View000

JEOLUSER 1/1

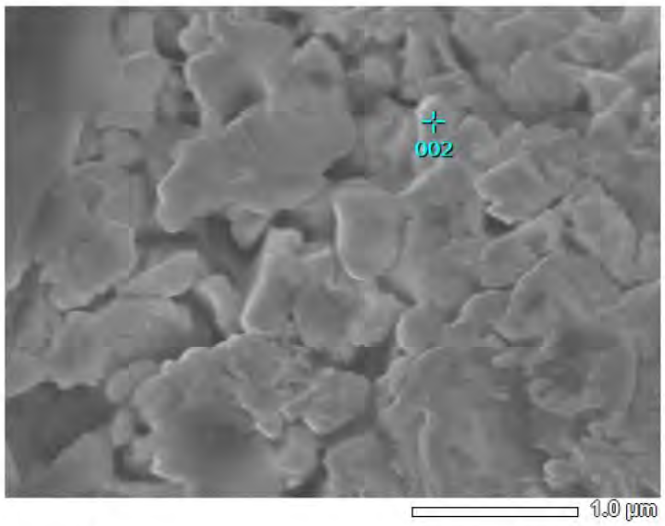


```
Title        : IMG1
-------------------------
Instrument   : 7600F
Volt         : 5.00 kV
Mag.         : x 30,000
Date         : 2017/12/09
Pixel        : 512 x 384
```

002 VFS = 1000 count

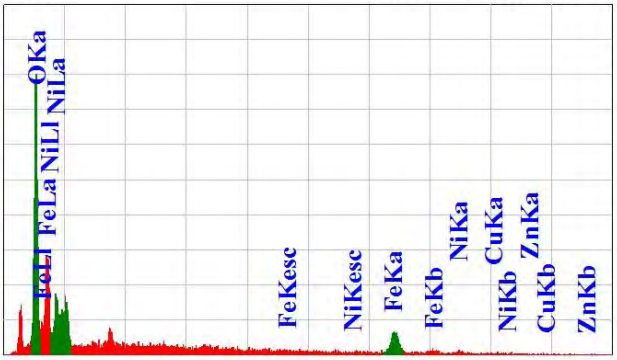


```
Acquisition Parameter
Instrument   : 7600F
Acc. Voltage : 10.0 kV
Probe Current: 1.00000 nA
PHA mode     : T3
Real Time    : 30.17 sec
Live Time    : 30.00 sec
Dead Time    : 0 %
Counting Rate: 785 cps
Energy Range :  0 - 20 keV
```

ZAF Method Standardless Quantitative Analysis
Fitting Coefficient : 0.1986

Element	(keV)	Mass%	Sigma	Atom%	Compound	Mass%	Cation	K
O K	0.525	28.72	0.37	59.43				40.5567
Fe K	6.398	37.19	1.70	22.05				41.7702
Ni L	0.851	20.91	0.94	11.79				10.0542
Cu L*	0.930	3.46	0.30	1.80				3.3057
Zn L	1.012	9.72	0.49	4.93				4.3132
Total		100.00		100.00				

JED-2300 AnalysisStation JEOL

Fig 4.7.2: EDS patterns at point 2 for x=0.00.

View000

JEOLUSER 1/1

Title : IMG1

Instrument : 7600F
Volt : 5.00 kV
Mag. : x 30,000
Date : 2017/12/09
Pixel : 512 x 384

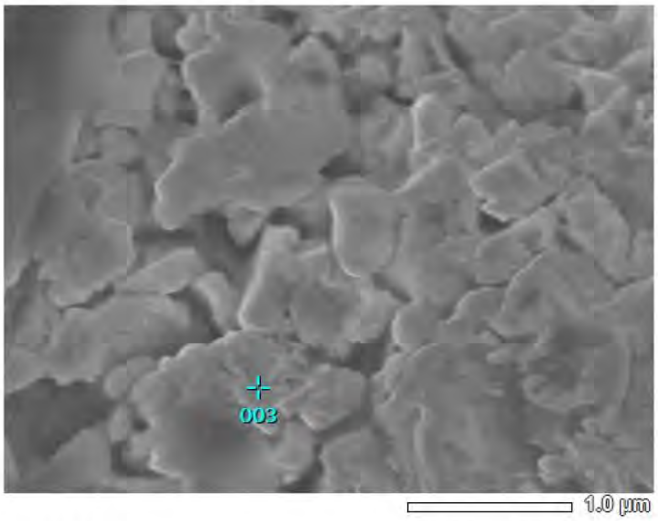

003 VFS = 1000 count

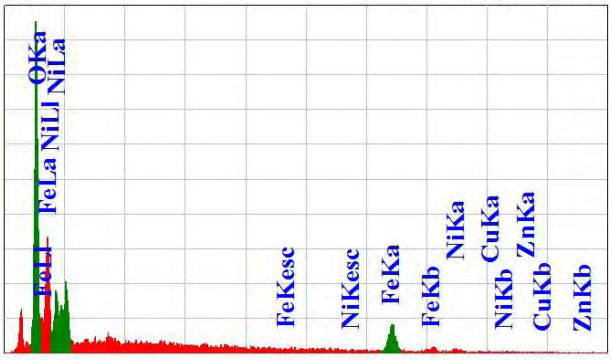

Acquisition Parameter
Instrument : 7600F
Acc. Voltage : 10.0 kV
Probe Current: 1.00000 nA
PHA mode : T3
Real Time : 30.23 sec
Live Time : 30.00 sec
Dead Time : 0 %
Counting Rate: 850 cps
Energy Range : 0 - 20 keV

ZAF Method Standardless Quantitative Analysis
Fitting Coefficient : 0.1593

Element	(keV)	Mass%	Sigma	Atom%	Compound	Mass%	Cation	K
O K	0.525	28.53	367945145087332190000.00	59.26				40.1784
Fe K	6.398	37.37	213832289534937030000.00	22.23				41.7895
Ni L	0.851	19.34	721192089103298990000.00	10.95				9.2829
Cu L*	0.930	4.15	193677073276649600000.00	2.17				4.0031
Zn L	1.012	10.61	431349142810011890000.00	5.39				4.7461
Total		100.00		100.00				

JED-2300 AnalysisStation JEOL

Fig 4.7.3: EDS patterns at point 3 for x=0.00.

View000

JEOLUSER 1/1

Title : IMG1

Instrument : 7600F
Volt : 5.00 kV
Mag. : x 30,000
Date : 2017/12/09
Pixel : 512 x 384

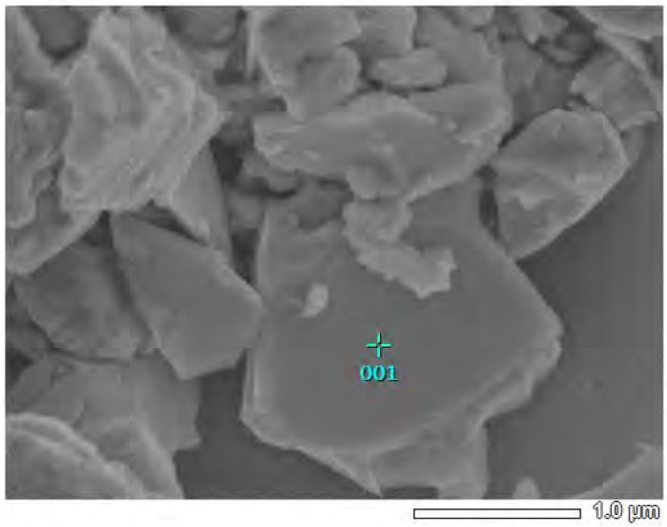

001 VFS = 1000 count

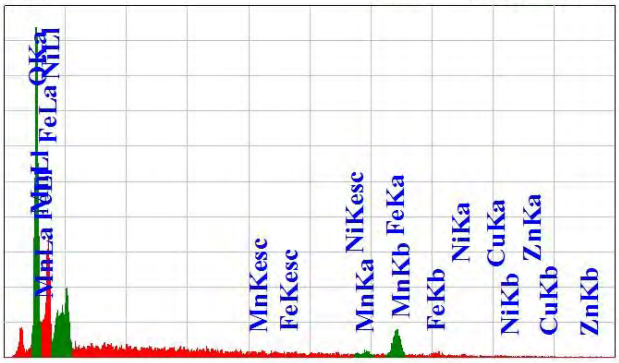

Acquisition Parameter
Instrument : 7600F
Acc. Voltage : 10.0 kV
Probe Current: 1.00000 nA
PHA mode : T3
Real Time : 30.21 sec
Live Time : 30.00 sec
Dead Time : 0 %
Counting Rate: 752 cps
Energy Range : 0 - 20 keV

ZAF Method Standardless Quantitative Analysis
Fitting Coefficient : 0.1430

Element	(keV)	Mass%	Sigma	Atom%	Compound	Mass%	Cation	K
O K	0.525	27.95	0.33	58.49				39.0293
Mn K*	5.894	2.50	0.46	1.52				2.6322
Fe K	6.398	38.67	1.60	23.18				42.2077
Ni L	0.851	15.94	0.79	9.09				7.2733
Cu L	0.930	4.35	0.26	2.29				4.1530
Zn L	1.012	10.58	0.44	5.42				4.7045
Total		100.00		100.00				

JED-2300 AnalysisStation JEOL

Fig 4.8.1: EDS patterns at point 1 for x=0.15.

View000

JEOLUSER 1/1

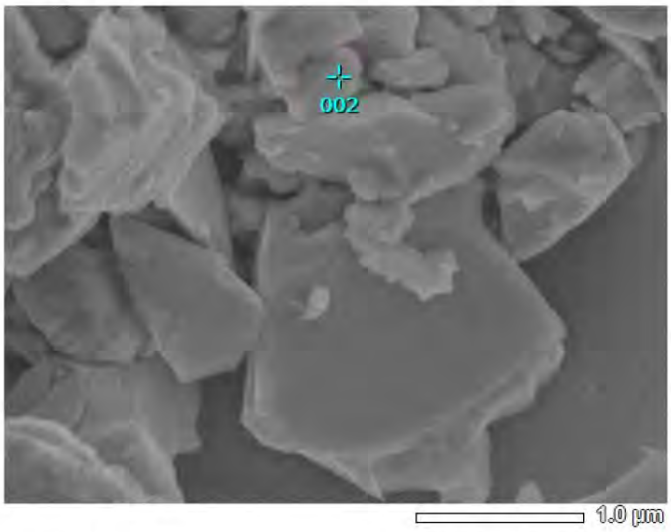


```
Title          : IMG1
----------------------------
Instrument     : 7600F
Volt           : 5.00 kV
Mag.           : x 30,000
Date           : 2017/12/09
Pixel          : 512 x 384
```

002 VFS = 1000 count

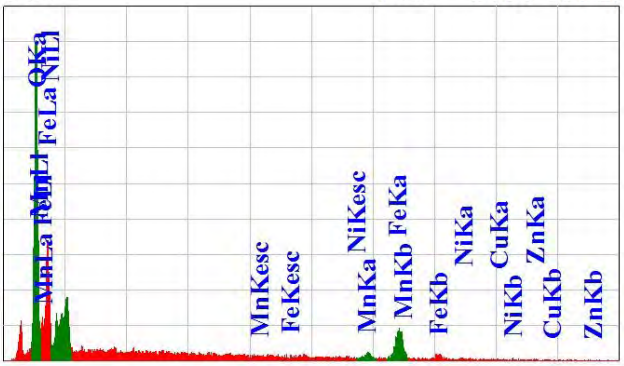


```
Acquisition Parameter
Instrument    : 7600F
Acc. Voltage  : 10.0 kV
Probe Current: 1.00000 nA
PHA mode      : T3
Real Time     : 30.22 sec
Live Time     : 30.00 sec
Dead Time     : 0 %
Counting Rate: 799 cps
Energy Range :  0 - 20 keV
```

ZAF Method Standardless Quantitative Analysis
Fitting Coefficient : 0.1596

Element	(keV)	Mass%	Sigma	Atom%	Compound	Mass%	Cation	K
O K	0.525	26.63	0.12	56.70				36.9915
Mn K*	5.894	5.84	0.58	3.62				6.0513
Fe K	6.398	40.59	1.63	24.76				43.4428
Ni L	0.851	14.04	0.76	8.15				6.0487
Cu L	0.930	3.72	0.25	1.99				3.4593
Zn L	1.012	9.18	0.41	4.78				4.0064
Total		100.00		100.00				

JED-2300 AnalysisStation JEOL

Fig 4.8.2: EDS patterns at point 2 for x=0.15.

View000

JEOLUSER 1/1

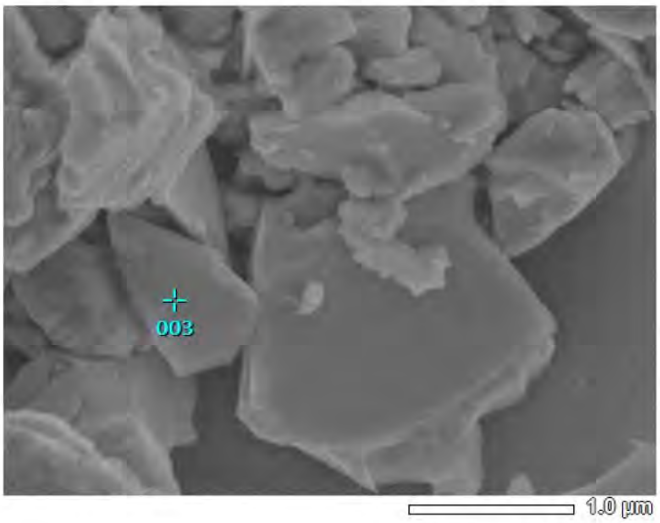

Title : IMG1

Instrument : 7600F
Volt : 5.00 kV
Mag. : x 30,000
Date : 2017/12/09
Pixel : 512 x 384

003 VFS = 1543 count

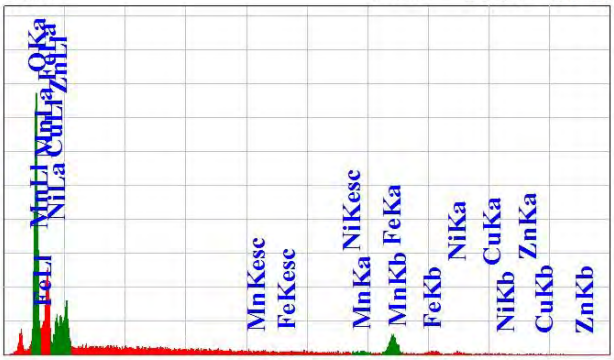

Acquisition Parameter
Instrument : 7600F
Acc. Voltage : 10.0 kV
Probe Current: 1.00000 nA
PHA mode : T3
Real Time : 30.24 sec
Live Time : 30.00 sec
Dead Time : 0 %
Counting Rate: 941 cps
Energy Range : 0 - 20 keV

ZAF Method Standardless Quantitative Analysis
Fitting Coefficient : 0.1221

Element	(keV)	Mass%	Sigma	Atom%	Compound	Mass%	Cation	K
O K	0.525	28.72	0.31	59.41				40.1366
Mn K*	5.894	2.60	0.42	1.57				2.7403
Fe K	6.398	37.27	1.46	22.09				40.7509
Ni L	0.851	16.82	0.74	9.48				7.7499
Cu L	0.930	4.21	0.25	2.20				4.0181
Zn L	1.012	10.37	0.41	5.25				4.6041
Total		100.00		100.00				

JED-2300 AnalysisStation JEOL

\

Fig 4.8.3: EDS patterns at point 3 for x=0.15.

Table 4.2: Mass of different elements in various samples of $(Ni_{0.4}Cu_{0.15}Zn_{0.45})_{1-x}Mn_xFe_2O_4$ sintered at 1100^0C

Composition	Elements	Point1 (%)	Point2 (%)	Point3 (%)	Expected (%)
$Ni_{0.4}Cu_{0.15}Zn_{0.45}Fe_2O_4$	Ni	23.94	20.91	19.34	9.85
	Cu	4.2	3.46	4.15	4
	Zn	11.34	9.72	10.61	12.35
	Mn	0	0	0	0
	Fe	34.77	37.19	37.37	46.90
	O	25.75	28.72	28.33	26.87
$Ni_{0.34}Cu_{0.1275}Zn_{0.3825}Mn_{0.15}Fe_2O_4$	Ni	15.94	14.04	16.82	8.42
	Cu	4.35	3.72	4.21	3.42
	Zn	10.58	9.18	10.37	10
	Mn	2.5	5.84	2.6	3.47
	Fe	38.67	40.59	37.27	47.13
	O	27.95	26.63	28.72	27

4.5. Complex Initial Permeability

The variation of complex permeability spectra for various samples of $(Ni_{0.4}Cu_{0.15}Zn_{0.45})_{1-x}Mn_xFe_2O_4$ sintered at 1100, 1150 and 1200^0C have been depicted in the figures 4.9, 4.10 and 4.11 respectively. The initial permeability ($\mu_i^{/}$) decreases with increasing Mn content which is shown in figure 4.8. The general characteristic spectra of the real part remain constant in a certain frequency range, but then drop sharply at higher frequencies to a very small values.

The decrease in permeability with increasing Mn^{2+} can be explained as the grain size has decreased. Permeability is greatly dependent on the internal structure of the composition on how the grain has grown, what kind porosity has been produced within the samples. The more Mn is added to the compositions, the grain size decreased which eventually resulted in lowering the permeability. The imaginary part ($\mu_i^{//}$) of the permeability spectra also have decreased with values of x.

The relative quality factor for various samples of $(Ni_{0.4}Cu_{0.15}Zn_{0.45})_{1-x}Mn_xFe_2O_4$ have been calculated from the loss factor for different sintering temperatures. This Q-factor is important for practical applications that indicates the measure of performance. Figure 4.10 shows the relative quality factor with increasing Mn^{2+} content for 1100, 1150 and 1200^0C sintering temperatures. In figure 4.11, permeability and relative quality factor for different values of x with varying temperature is given. It is noticed that RQF is high for $(Ni_{0.4}Cu_{0.15}Zn_{0.45})_{1-x}Mn_xFe_2O_4$ in the absence of Mn at 1200^0C. At higher frequency, a sudden increase in permeability is noticed after a continuation of stability. This frequency is known as natural resonance frequency beyond which the permeability takes a sharp fall. This is common for all the values of x in every temperatures.

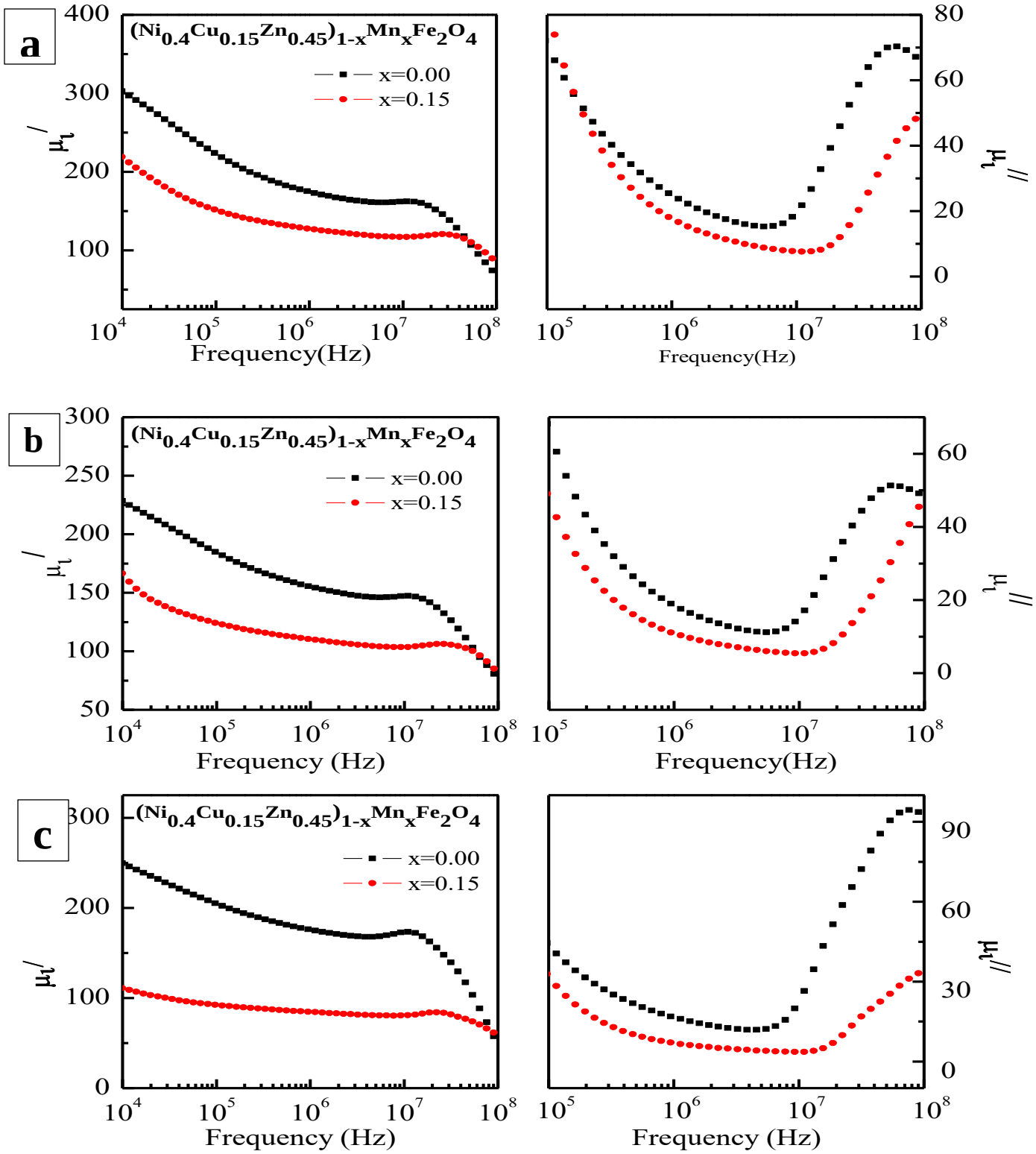

Figure 4.9: The real and imaginary part of permeability spectrum for $(Ni_{0.4}Cu_{0.15}Zn_{0.45})_{1-x}Mn_xFe_2O_4$ sintered at (a) 1100 (b) 1150 and (c) 1200^0C in air.

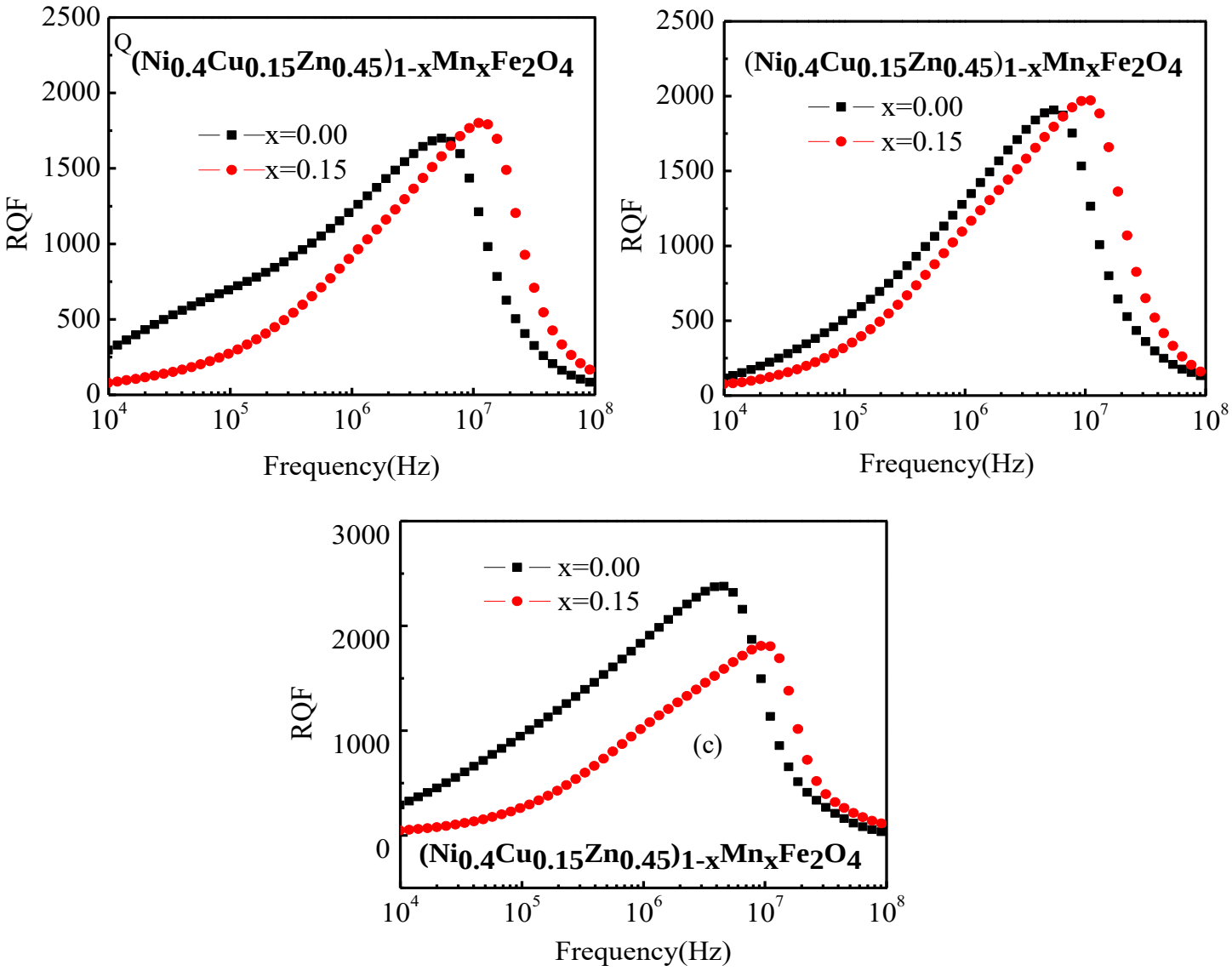

Figure 4.10: Relative quality factor (RQF) of permeability spectrum for $(Ni_{0.4}Cu_{0.15}Zn_{0.45})_{1-x}Mn_xFe_2O_4$ sintered at (a) 1100 (b) 1150 and (c) 1200^0C in air.

The decrease in permeability with increasing sintering temperature given in figure 4.11 can be explained in terms of porosity and density. As seen from figure 4.5 the bulk density decreases and also the porosity increases when the sintering temperature rises. Pores affect the moments of domains that tend to align along the direction of applied magnetic field. It is found that bulk density of the sample is a linear function of grain size. The μ_i' is dependent on both the domain wall

susceptibility and intrinsic rotational susceptibility. The domain wall susceptibility is affected by the grain size. As the grain size decreases, the permeability also falls with it.

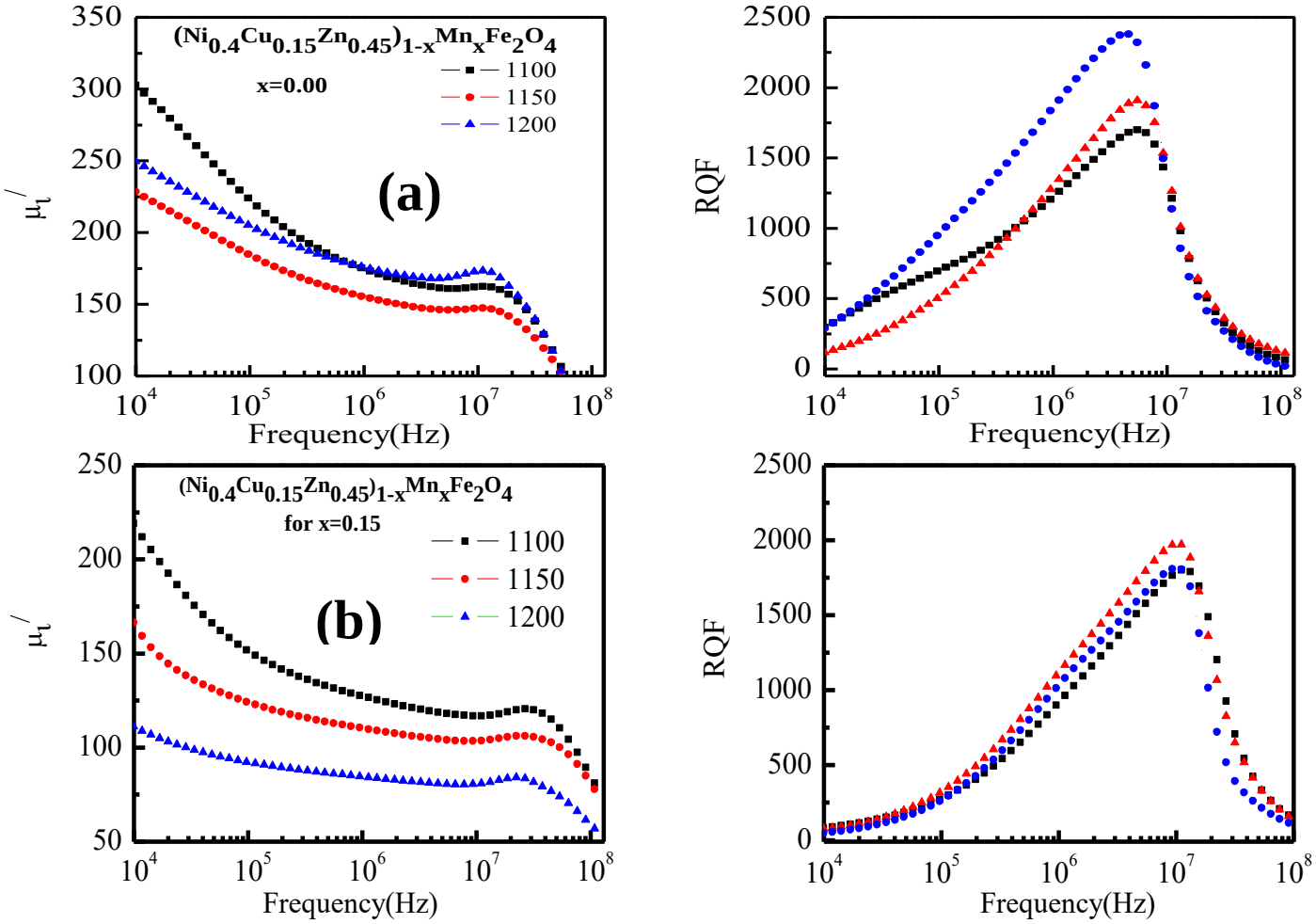

Figure 4.11. The real part and relative quality factor of permeability spectrum for $(Ni_{0.4}Cu_{0.15}Zn_{0.45})_{1-x}Mn_xFe_2O_4$ for (a) x=0.00, (b) x=0.15 .

CHAPTER 5

Conclusions

Polycrystalline $(Ni_{0.4}Cu_{0.15}Zn_{0.45})_{1-x}Mn_xFe_2O_4$ ferrite is successfully prepared by solid state reaction method. The XRD patterns clearly indicate their single phase and formation of spinel structure. Lattice parameter a_o, increases with increase of Mn^{2+} content in $(Ni_{0.4}Cu_{0.15}Zn_{0.45})_{1-x}Mn_xFe_2O_4$. This is due to, Mn^{2+} has an ionic radius of 0.83 Å which replaces Zn^{2+} (0.74 Å), Ni^{2+} (0.69Å) and Cu^{2+} (0.72Å). It is also observed that bulk density and theoretical density decreases with increasing porosity which may have resulted from the replacement of heavier elements (Ni, Zn, Cu have atomic weight of 58.6934(amu), 65.38(amu), 63.546(amu) respectively) with comparatively lighter element (Mn has atomic weight of 54.938 (amu)). The grain size has decreased with increasing Mn content due to porosity. When samples were cooled down, each composition attained completely different physical and chemical properties due to different melting points for different elements that eventually affected the grain size. The EDS result shows the homogeneity of elements in the samples. The initial permeability (μ_i') decreases with increasing Mn^{2+} content for temperature 1100, 1150 and 1200^0C. The general characteristic spectra of the real part remain constant in a certain frequency range, but then fall at higher frequencies to a very small values. The resonant frequency f_r also increases with increasing Mn^{2+} content. RQF value found to be the highest for $(Ni_{0.4}Cu_{0.15}Zn_{0.45})_{1-x}Mn_xFe_2O_4$ in the absence of Mn at 1200^0C.

Recommendations for Future Research

1. More samples of each composition could be produced for each value of x .this would have enhanced the accuracy of the results reducing the error margin.

2. More values of x could have been taken for enhanced demonstration of the ferrite characteristics.

3. More methods for characterizing the produced samples could have been equipped for greater understanding and analyses.

4. The process of ball milling could have been used instead of hand milling. This would have resulted in lesser amount of human errors, including better homogenous distribution of the materials in the mixture.

5. Lower calcination and sintering temperature should have been taken.

6. Magnetization and SEM of each sample should have been done for better understanding the permeability spectra.

References

[1] Winter Science. *Application of Ferrites*. Available from http://winnerscience.com/2011/03/30/applications-of-ferrites/ [7th October 2017]

[2] Carl DW, Mark JC, John KT, Erik RS. *Implantable Medical Device.* Google PatentWO2007112044 A2.04-10-07.

[3] The Engineering Toolbox. *Permeability: Electromagnetism and Formation of Magnetic Fields*. Available from: https://www.engineeringtoolbox.com/permeability-d_1923.html [7th October 2017]

[4] Job B. *Quora:What is the Magnetic Permeability of Zinc?* Available from: https://www.quora.com/What-is-the-magnetic-permeability-of-Zinc [7th October 2017]

[5] Gawas, UB, Verenkar VMS, Meena SS. *Influence of Mn Substitution on Mossbauer and Magnetic Properties of Ni-Zn Ferrite Nanoparticles.*2017. Available from: https://doi.org/10.1007/s10948-017-4149-7 [9th October 2017]

[6] Akther Hossain AKM, Biswas TS, Mahmud ST, Takeshi YHT, Tomoji K. *Enhancement of Initial Permeability Due to Mn Substitution in Polycrystalline* $Ni_{0.50-x}Mn_x\ Zn_{0.50}Fe_2O_4$. 2009. Available from: https://doi.org/10.1016/j.jmmm.2008.08.059[9th October 2017]

[7] Roy PK, Bera J. *Effect of Mg Substitution on Electromagnetic Properties of* $(Ni_{0.25}Cu_{0.20}Zn_{0.55})\ Fe_2O_4$ *Ferrite Prepared by Auto Combustion Method.* 2006. Available from: https://doi.org/10.1016/j.jmmm.2005.03.007[10th October 2017]

[8] Nazrul I. *Investigation of Structural and Magnetic Properties of Gd Substituted Mn-Ni-Zn Ferrites.*2013. Availablefrom:http://lib.buet.ac.bd:8080/xmlui/bitstream/handle/123456789/4384/Full%20Thesis.pdf?sequence=1&isAllowed=y[11th October 2017]

[9] Pradeep A, Chandrasekaran G. *FTIR study of Ni, Cu and Zn Substituted Nano-Particles of* $MgFe_2O_4$. 2006. Available from: https://doi.org/10.1016/j.matlet.2005.08.053[11th October 2017]

[10] Lucas A, Lebourgeois R,Mazaleyrat F, Laboure E. *Temperature Dependence of Core Loss in Cobalt Substituted Ni–Zn–Cu ferrites*.2011. Available from: https://doi.org/10.1016/j.jmmm.2010.10.037[12th October 2017]

[11] Dasan YK, Guan BH, Zahari MH and Chuan LK. ***Influence of La 3+ Substitution on Structure, Morphology and Magnetic Properties of Nanocrystalline Ni-ZnFerrite.*** 2017. Available from: https://doi.org/10.1371/journal.pone.0170075[13th October 2017]

[12] Stijntjes, Theo & van Loon, Bob. *Early Investigations on Ferrite Magnetic Materials by J. L. Snoek and Colleagues of the Philips Research Laboratories Eindhoven*. 2008. Proceedings of the IEEE. 96. 900-904. 10.1109/JPROC.2008.917767.Availablefrom:https://www.researchgate.net/publication/2998518_Early_Investigations_on_Ferrite_Magnetic_Materials_by_J_L_Snoek_and_Colleagues_of_the_Philips_Research_Laboratories_Eindhoven[14th October 2017]

[13] Singh A, Singh J, Disanjh HS. *Synthesis of Pure and Mixed Nickel-Cobalt Ferrites (Ni1-XCoXFe2O4) by Combustion Method and Characterization* .2015. Available from: http://www.jocpr.com/articles/synthesis-of-pure-and-mixed-nickelcobalt-ferrites-ni1xcoxfe2o4-bycombustion-method-and-characterization.pdf [17th October 2017]

[14] Rashid M, Kabir H, Rahaman M, Gafur A, Jamil ATMK and Ahmed SJ. *Investigation of Structural, Dielectric, and Electrical properties of Zn-substituted Li-Ni ferrite*. 2015. Available from: DOI : 10.9790/4861-07517683 [18th October 2017]

[15] AdiChemistry. *Spinel and Inverse Spinel Structures*. Available from: http://www.adichemistry.com/inorganic/cochem/spinels/spinel-structures.html [20th October 2017]

[16] Bland J. *CMP:Temperature Dependence.* 2003. Available from: http://www.cmp.liv.ac.uk/frink/thesis/thesis/node40.html[21st October 2017]

[17] Kullabs. *Note on Classification of Magnetic Material*. Available from: https://www.kullabs.com/classes/subjects/units/lessons/notes/note-detail/3067 [21st October 2017]

[18] University of Birmingham. *Classification of Magnetic Materials*. Available from: https://www.birmingham.ac.uk/Documents/college-eps/metallurgy/research/Magnetic-Materials-Background/Magnetic-Materials-Background-4-Classification-of-Magnetic-Materials.pdf[21st October 2017]

[19] Chikazumi S. *Physics of Magnetism.*1964.

[20] Hadfield D. *Permanent Magnets and Magnetism.* 1962.

[21] Cullity BD. *Introduction to Magnetic Material.* 2009.

[22] Sikder SS. *Temperature Dependence of Magnetization and Induced Magnetic Anisotropy of Some Fe, Co and Ni-based Amorphous Ribbons*. Ph. D. Thesis BUET Bangladesh. 1999.

[23] Hussain KMA. *Study of Complex Permeability and Secondary Effects in Some Cobalt and Manganese Based Ferrites.* M. Phil. Thesis BUET Bangladesh. 2003.

[24] Kittel C. *Introduction to Solid State Physics*, 7th edition, Jhon Wiley & Sons, Inc., Singapore. 1996.

[25] Akther Hossain AKM, Seki M, Kawai T and Tabata H. *Colossal Magnetoresistance in Spinel type* $Zn_{1-x}Ni_xFe_2O_4$*, J. Appl. Phys.*2004.

[26] Goldman A. *Handbook of Modern Ferromagnetic Materials*, Kulwer Acad. Pub, Boston, U.S.A. 1999.

[27] Valenzuela R. *Magnetic Ceramics*, Cambridge University Press, Cambridge. 1994.

[28] Kingery WD, Bowen HK and Uhlman DR. *Introduction to Ceramics*, 2nd edition, Wiley Interscience, Newyork, pp. 476. 1976.

[29] Coble RL and Burke JE. *4th Int. Symp. On the Reactivity of Solids*, Amsterdam, pp. 38-51. 1960.

[30] I. McColm J and Clark M. *Forming, Shaping and Working of high Performance Ceramics*, Blackie, Glasgow, pp. 1-338. 1988.

[31] Akhter Hossain AKM, Rahman ML. *Enhancement of Microstructure and Initial Permeability Due to Cu Substitution in* $Ni_{0.50-x}Cu_xZn_{0.50}Fe_2O_4$ *Ferrites*.2011.

[32] Tapdiya S, Shrivastava AK., Singh S. *Effect of Mn Substitution on Structural and Magnetic Properties of Cobalt Ferrite*.2017.

[33] Akhter Hossain AKM , Kabir KK ,Seki M, Kawai T, Tabata H. *Structural, AC and DC Magnetic Properties of* $Zn_{1-x}Co_xFe_2O_4$ .2007.

[34] Khan MHR, Akther Hossain AKM. *Reentrant Spin Glass Behavior and Large Initial Permeability of* $Co_{0.5-x}Mn_xZn_{0.5}Fe_2O_4$. 2012.

[35] Periodic Table Of The Elements . *Zinc Melting points*. Available from: https://www.cs.colorado.edu/~kena/classes/7818/f01/assignments/pt.html [4th December 2017]